EXTENSION OF THE LATE HOLOCENE SEA-LEVEL RECORD IN NORTH CAROLINA, USA

Jessica Kegel

April 2015

Director of thesis: Dr. Stephen J. Culver

Major Department: Geological Sciences

Future sea-level rise will dramatically affect coastal landscapes and populations. The coast of North Carolina (USA) is particularly vulnerable to sea-level rise because its low-lying coastal plain is expansive, has a low gradient, provides significant ecosystem services and is economically important. In order to understand how future sea-level rise may affect the coast, it is necessary to study past sea-level rise. Widespread salt-marshes compose much of North Carolina's coastal system, providing an excellent environment from which to produce relative sea-level reconstructions using salt-marsh foraminifera, whose distribution is controlled by tidal elevation. Distinctive assemblage zones related to different tidal ranges can be recognized in salt-marsh foraminiferal assemblages, allowing them to be used as a proxy for reconstructing sea level as sea-level indicators.

Foraminiferal assemblages from surface samples along two transects at Sand Hill Point on Cedar Island, North Carolina added to an existing modern training set of paired observations of foraminiferal assemblages and tidal elevation; these data provide local analogues for interpreting fossil assemblages using a locally weighted-weighted average (LWWA) regression model. Foraminiferal assemblages preserved in a radiocarbon-dated core of salt-marsh peat from Sand Hill Point were used to produce a continuous, high-resolution late Holocene relative sea-level reconstruction.

The existing late Holocene RSL reconstruction from North Carolina is based on two sites: Sand Point on Roanoke Island and Tump Point on Cedar Island. The Sand Point record spans the last ~2200 years, but the Tump Point record spans only the last ~1000 years. Therefore, the sea-level history described from 200 BC to 1000 AD is based on only one site. The new sea-level reconstruction from Sand Hill Point extends the existing record from nearby Tump Point, NC by 1400 years, producing a high resolution, continuous record of sea-level change spanning 1500 BC – 1915 AD. This new record tests whether patterns and rates of late Holocene sea-level changes reconstructed elsewhere in North Carolina are consistent throughout the region. The calculated average rate of relative sea-level rise for Sand Hill Point of 0.7 mm/year is consistent with patterns of regional rates along the US Atlantic coast, which may be partly attributed to isostatic response to deglaciation of the Laurentide Ice Sheet.

EXTENSION OF THE LATE HOLOCENE SEA-LEVEL RECORD IN NORTH CAROLINA, USA

A Thesis

Presented to the Faculty of the Department of Geological Sciences

East Carolina University

In Partial Fulfillment of the Requirements for the Degree

Master of Science in Geological Sciences

By

Jessica Kegel

April, 2015

EXTENSION OF THE LATE HOLOCENE SEA-LEVEL RECORD IN NORTH CAROLINA, USA

By

Jessica Kegel

APPROVED BY:

DIRECTOR OF THESIS: _____

Stephen J. Culver

COMMITTEE MEMBER: _____

Eduardo Leorri

COMMITTEE MEMBER: _____

David Mallinson

EXTERNAL COMMITTEE MEMBER: _____

Andrew Kemp

CHAIR OF THE DEPARTMENT OF GEOLOGICAL SCIENCES: _____

Stephen J. Culver

DEAN OF THE GRADUATE SCHOOL: _____

Dr. Paul Gemperline

ACKNOWLEDGEMENTS

I would like to thank my advisor Steve Culver for his unwavering support and encouragement as well as my committee members, Eduard Leorri, Dave Mallinson and Andrew Kemp, for their guidance and wisdom. For their help in the field, with the writing process and gracious input into this project I would like to thank Don Barber, Christopher Bernhardt, Ben Horton, Jim Morrison and Anna Lee Woodson. Without the support and confidence of my parents, family and friends this would not have been possible. I would also like to acknowledge that this work was made possible by National Science Foundation (NSF) grant EAR - 1322742.

TABLE OF CONTENTS

LIST OF TABLES

LIST OF FIGURES

INTRODUCTION

Sea-level rise has the potential to affect every coastal marsh on the planet (Gunnell et al., 2013) and relative sea-level (RSL) reconstructions provide a context for current trends and insight into the likely effects of predicted future change. Salt-marsh foraminifera are abundant and their distribution is controlled by the tidal elevation (Scott and Medioli, 1978; 1980), making them an important tool in paleoenvironmental, including RSL, reconstructions. Generally, at decadal to centennial time scales, salt-marshes accumulate sediment, maintaining their elevation, in response to changes in sea level. When the rate of sea-level rise exceeds the rate of accretion, the tidal elevation of the marsh decreases. When accumulation exceeds sea-level rise, the elevation in relation to the tidal frame of the marsh increases. These changes impact the sedimentological processes and the plant distribution and are recorded by the foraminiferal assemblages over time (e.g., Scott and Medioli, 1978, 1980; Gehrels, 1994; Horton, 1999).

The most common plants in eastern North Carolina salt-marshes are *Juncus roemerianus*, *Distichlis spicata,* and *Spartina alterniflora.* Known as black needlerush, *Juncus roemerianus* is a major structural component of marshes (Christian et al., 1990). It is a stress-tolerant plant typically associated with high marsh settings. *Distichlis spicata*, also known as saltgrass, is an upright grass that is often associated with high marsh settings, occurring in patches across the marsh. *Spartina alterniflora,* often known as cordgrass, grows on the seaward edge of salt-marshes. These plants differ in their ecological preferences and tolerance to inundation by saltwater (Christian et al., 1990). Tidal-marsh plants are adapted to anaerobic conditions, even during submergence. These marsh plants grow from rhizomes, a rootstock from which hundreds of vertical stems may be supported. After death these rhizomes, as well as leaves, seeds, etc.,

might remain in growth position (Kemp et al., 2013a) and, when conditions allow for preservation, may be used for accurately dating former tidal-marsh surfaces.

In order to reconstruct sea-level changes during the Holocene from salt-marsh deposits, a transfer function is commonly used (e.g., Edwards and Horton, 2000; Gehrels, 2000; Horton and Edwards, 2006; Massey et al., 2006; Horton and Culver, 2008; Leorri et al., 2008; Kemp et al., 2009b, 2011; Leorri et al., 2010; Juggins and Birks, 2012). A transfer function offers a robust methodology for paleoenvironmental reconstructions via an understanding of the relationship between modern organisms and an environmental variable. A linear regression or unimodal approach can be taken depending on the relationship of the organism to the environmental variable. Foraminifera most often display a unimodal distribution with tidal elevation, few species display a relative abundance which increases or decreases linearly (Kemp and Telford, 2015). The recently developed locally weighted-weighted average (LWWA) regression model has proven to be a useful transfer function approach which can balance the precision of a small, local dataset with the diversity of a large, regional training set for reconstructing relative sea-level rise during the Holocene (e.g., Juggins and Birks, 2012; Kemp and Telford, 2015).

Foraminiferal assemblage data from Sand Hill Point on Cedar Island, North Carolina (Figure 1) are used here to develop a new transfer function, temporally extend the current sea-level record from Tump Point (Kemp et al., 2011; Figure 1), and produce a continuous, high resolution reconstruction of relative sea level change during the late Holocene. The new combined Tump Point and Sand Hill Point sea-level record will be compared to previously documented rates of sea-level change along the US Atlantic coast to help determine whether relative sea-level changes in Pamlico Sound during the late Holocene are consistent with regional trends.

Figure 1: Map of the study area, Sand Hill Point on Cedar Island, North Carolina, including the 10 sites in the regional foraminiferal dataset (Kemp et al., 2009a) and the four active inlets.

REGIONAL SETTING

ALBEMARLE-PAMLICO ESTUARINE SYSTEM

The North Carolina coastal system can be divided into southern and northern zones. The northern zone is characterized by a gentle slope, long barrier islands with few inlets, and drowned-river valleys whereas the southern zone is characterized by short barrier islands with many inlets and narrow back-barrier estuaries (Riggs et al., 2008). The estuaries of the northern zone formed when rising relative sea-level flooded the paleo-drainage network consisting of the paleo-valleys of the Roanoke, Tar/Pamlico and Neuse Rivers. They act as mixing basins where variations in salinity largely determine the nature and distribution of salt-marsh plant communities (Riggs et al., 2008).

The Albemarle-Pamlico estuarine system (APES) is the second largest estuary system in the contiguous United States, covering an area of about 4,350 km^2, occurs in the northern zone. The APES consists of a system of drowned river valleys connected to the Atlantic Ocean through four inlets in the Outer Banks barrier islands: Oregon Inlet, Hatteras Inlet, Ocracoke Inlet and Drum Inlet. These inlets, along with river input, control the salinity and sedimentation of the system. The main sources of freshwater into Pamlico Sound are the Tar-Pamlico and Neuse rivers (Wells and Kim, 1989).

The APES is a microtidal system sensitive to changes in sea-level (Kemp et al., 2009a). The system has a maximum tidal range of ~1 m near the inlets which decreases to only ~10 cm or less throughout much of the APES region (Wells and Kim, 1989), including just 11 cm at Cedar Island (tidesandcurrents.noaa.gov). This results in a system with generally wind-driven tides and negligible astronomical tides.

CEDAR ISLAND

The study area, Cedar Island (Figure 1), is located in southern Pamlico Sound where thick, continuous accumulations of salt-marsh peat have been observed (e.g., Kemp et al., 2009a; Woodson, 2012). The topographical relief is extremely low, resulting in some parts of the marsh being flooded much of the time (Christian et al., 1990).

Salt-marshes often display a vertical zonation of plants (Appendix I) and are characterized by a low diversity of vegetative zones (Woerner and Hackney, 1997) controlled by elevation. *Juncus roemerianus* is the major plant component at Cedar Island, decreasing in relative abundance from the marsh edge inland (Christian et al., 1990), but generally dominating the entire salt-marshsurface. *Juncus roemerianus* is a marsh plant which occurs over a wide range of physical and chemical variables including salinity, elevation and percent organic matter (Woerner and Hackney, 1997). The Cedar Island marsh seaward edge tends to be bordered by *Spartina alterniflora. Distichlis spicata* is also fairly common at Cedar Island. Spatially across the marsh, from the water edge to the mainland, vegetative zones tend to shift from a small border of *Spartina alterniflora* at the marsh edge to an overwhelmingly dominant zone of *Juncus roemerianus* with patches of *Distichlis spicata.*

PREVIOUS WORKS

SALT-MARSH FORAMINIFERA AS SEA-LEVEL INDICATORS

Salt-marsh foraminiferal distributions in Nova Scotian marshes were documented by Scott and Medioli (1978, 1980). Their work validated the observed relationship, previously documented for salt-marsh plants, between marsh foraminifera and elevation (e.g., Phleger, 1965, 1970). The authors utilized the same techniques as those used in a California-based study (Scott, 1976) in order to compare results and form a comprehensive picture of the vertical distribution of marsh foraminifera. Despite differences in salinity, tidal range, and climate between study sites, the foraminiferal assemblages proved to be remarkably similar. Their data suggested a strong correlation between tidal elevation (above mean sea level) and marsh foraminiferal zones, meaning that salt-marsh foraminifera may be used as sea-level indicators (Appendix I). Since the pioneering work of Scott and Medioli (1978, 1980), the applicability of marsh foraminifera as sea-level indicators has been documented worldwide (e.g., Horton, 1999; Gehrels, 2000; Gehrels et al., 2004; Horton and Edwards, 2006; Southall et al., 2006; Leorri et al., 2010; Callard et al., 2011)

The relationship between modern foraminiferal assemblages, modern plant communities and tidal elevations along the coast of Maine were used (Gehrels, 1994) to test the hypothesis that using assemblages of fossilized salt-marsh foraminifera as sea-level indicators improves the precision of local sea-level studies compared to marsh plant indicators. The study found foraminifera to be excellent sea-level indicators due to low species diversity and narrow modern vertical ranges, as compared to previously utilized salt-marsh vegetative zones.

The potential use of foraminifera in more precise reconstructions of Holocene sea-level change was supported by documenting the relationship between foraminiferal distributions and a

range of environmental variables including flooding frequency, salinity, substrate, pH, and vegetation cover (Horton, 1999). Horton (1999) found that the surface death assemblages (modern assemblage counts excluding foraminifera presumably live at the time of collection) indicated that the assemblages were in equilibrium with the depositional environment in which they were found, reducing the impact of seasonal assemblage changes. Building upon the work of Shennan (1982) in Fenland, England, Horton (1999) noted that the understanding of former sea levels based on the identification and interpretation of foraminiferal assemblages, requires that the indicative meaning, the vertical relationship of the local environment in which the assemblage accumulated to a reference tide level, is known.

FORAMINIFERA-BASED TRANSFER FUNCTIONS FOR SEA-LEVEL RECONSTRUCTIONS

The transfer function is a statistical approach which quantifies the relationship between the environmental variable of interest (elevation as a proxy for tidal flooding) and the environmental proxy (foraminifera), so that the former may be expressed as a function of the latter (Imbrie and Kipp, 1971). The transfer function approach was used for the first time to estimate paleoelevation in marsh samples as evidence for coseismic subsidence related to a large earthquake on Vancouver Island (Guilbault et al., 1996). Modern salt-marsh foraminiferal assemblages were used and a transfer function was applied to calculate the paleoelevations of fossil samples. The study was able to estimate coseismic submergence using statistical analysis of foraminiferal data.

In the UK, the vertical distribution of foraminifera was used for a quantitative assessment of relative sea-level by Horton et al. (1999a). Salt-marsh foraminifera were collected from ten coastal sites in the UK and zones were defined based on cluster analyses of assemblages. Following the methodology of Shennan (1986), the indicative meaning was determined and the

elevation of each station was expressed as a standardized water level index (SWLI) in order to compare between sites. Strong vertical zonations were revealed and foraminiferal assemblages were separated into high- and middle-marsh zones. Horton et al. (1999a) suggested that a possible way to utilize the relationship between foraminiferal assemblages and elevation is to develop a transfer function for sea-level studies.

A foraminiferal-based transfer function was developed using a weighted average (WA) regression model and evaluated in terms of the root-mean square error of prediction (RMSEP) and applied to salt-marsh foraminiferal assemblages in a core from the UK (Horton et al. 1999b). The results supported the concept that the distribution of foraminifera in the intertidal zone is a function of elevation. The statistical performance measurements suggested that precise reconstructions of former sea-level are possible. Horton et al. (1999b) concluded that transfer functions are an important tool in reconstructing sea-level changes and also provide a means to produce sea-level index points

Similarly, Gehrels (2000) developed a foraminifera-based transfer function to produce a high-resolution sea-level record from salt-marsh deposits in Maine. The transfer function was applied to cores from two marshes and validated against local tide-gauge data. Gehrels (2000) noted that a large training set is required to obtain a reliable transfer function for calculating the indicative meaning of fossil samples and that the most accurate sea-level records are those obtained from salt-marsh peat sequences which are home to foraminifera with optimum occurrences in the middle of the flooding duration gradient. Gehrels (2000) concluded that the transfer function approach offered great potential for obtaining high-resolution (decadal-scale) records of sea-level.

A compilation of surface foraminiferal studies was used (Horton and Edwards, 2006) in order to assess the significance of a foraminifera-based transfer function which would be capable of producing high-resolution records of sea-level change. Horton and Edwards (2006) expanded on previous distributional studies (e.g., Horton, 1999) and suggested that when the whole intertidal zone is used to gather surficial foraminiferal data, the dead surficial assemblage is the most appropriate for sea-level studies. More importantly, the work solidified the effectiveness of foraminiferal assemblages as proxies for elevation, allowing for the use of foraminiferal-based transfer functions to reconstruct relative sea-level changes. Horton and Edwards (2006) indicated that the combination of intertidal foraminiferal data and the transfer function approach offers a number of distinct advantages for paleoenvironmental reconstruction including the expanded range of "useful" intertidal sediments, reconstructions with quantified error terms, replicable methodology and improved record comparability.

SALT-MARSH FORAMINIFERAL DISTRIBUTION IN NORTH CAROLINA

The relationship between foraminifera and elevation was documented (Horton and Culver, 2008) from three back-barrier sites on the Outer Banks, North Carolina. The study aimed to provide a better understanding of the relationship between foraminifera and sea level by identifying site-specific and regional patterns of modern foraminiferal distributions across the three North Carolina sites. Following the methods of Horton and Edwards (2006), Horton and Culver (2008) also described the relationship between foraminiferal distribution with flooding frequency, pH, salinity, substrate, and vegetation cover across all three sites. The study was the first to be done in a salt-marsh environment dominated by wind-driven tides, where astronomical tides are negligible. Horton and Culver (2008) documented 13 to 21 dead foraminiferal species in surface samples and foraminiferal zones were determined for each of the three sites. They

suggested that the distribution of foraminifera in the intertidal zone is usually a direct function of elevation, but note that all available environmental variables, except pH, play a role in determining foraminiferal distributions.

Salt-marsh foraminifera were further documented in North Carolina (Kemp et al., 2009a) to form the basis for reconstructions of paleoenvironmental change. Kemp et al. (2009a) identified elevation-dependent ecological zones at ten sites within the APES, adding to the dataset of Horton and Culver (2008) for a total of 145 surface samples. All sites showed a clear vertical zonation of foraminiferal assemblages except for Tump Point (Figure 1). The samples from this site were all dominated by the same assemblage, *Miliammina fusca* (30% to 70%) and *Tiphotrocha comprimata* (8–34%), due to the limited elevation range of 0.1m (Kemp et al., 2009a). The study determined that salt-marsh foraminifera from the APES are appropriate to use as accurate indicators of sea-level changes and that datasets from multiple salt-marsh settings are the most useful for North Carolina Holocene sea-level reconstructions due to the varying spatial trends of foraminiferal assemblage zones across the region.

Since using salt-marsh foraminifera as sea-level indicators requires an understanding of the vertical distribution of living foraminifera, it is important to document their infaunal distribution in a variety of settings and geographic locations. Culver and Horton (2005) suggested that this is important when making sea-level interpretations from the foraminifera contained in cored salt-marsh deposits. The study documented the depth distribution of both live and dead foraminifera in salt-marsh cores from North Carolina and compared them with the results of other salt-marsh studies in North America. This led to the determination that infaunal foraminifera in North Carolina marshes generally do not live as deep as in other marshes,

indicating that the assemblages of foraminifera found in the 0 – 1 cm sediment interval in North Carolina marshes can serve as the model to relate older marsh deposits to sea-level change.

NORTH CAROLINA SEA-LEVEL RECORD

Horton et al. (2009) and Engelhart and Horton (2013) compiled existing and new relative sea-level data to produce a comprehensive database for North Carolina, yielding new sea-level index points and comparing the database to a glacial isostatic adjustment (GIA) model. The database indicated a need to extend the observational data into the early Holocene where few data points exist. Comparison of the database to a dynamic GIA model and with local tide-gauge data suggested an additional increase of mean sea-level rise of 2 mm/year during the late twentieth century.

Kemp et al. (2009b) reconstructed sea-level changes since 1500 AD using data from two North Carolina salt-marshes, Tump Point in southern Pamlico Sound and Sand Point, ~120 km to the north, on the margin of Croatan Sound (Figure 1). The study aimed to identify the timing and magnitude of recent accelerated relative sea-level rise, previously documented elsewhere (e.g., Gehrels et al., 2005; Church and White, 2006; Horton et al., 2009; Woodworth et al., 2009). Transfer functions were used to reconstruct relative sea level using modern elevation data from foraminiferal assemblages across the North Carolina marshes identified by Kemp et al. (2009a). The transfer function was applied to core samples from Sand Point and Tump Point and the reconstruction was validated against regional twentieth century tide gauges. Sand Point and Tump Point proved to be ideal settings for producing high-resolution records because thick sequences of marsh sediment present in the microtidal system reduced the vertical uncertainty of the late Holocene sea-level estimations. The regional reconstruction dated back to 1500 AD and

identified a 2.2 mm/year increase in the rate of relative sea-level rise, beginning between 1879 and 1915 AD (Kemp, 2009; Kemp et al., 2009b, 2011).

The dataset of modern foraminifera from North Carolina was used and the same transfer function was applied to additional deeper samples from the Sand Point and Tump Point cores in order to reconstruct relative sea level for the past 2100 years (Kemp et al., 2011). Nearly identical relative sea-level curves for the two sites suggested that local-scale factors including tidal-range change and sediment compaction were not important influences on relative sea-level change in the region over the past two millennia. The records were corrected for vertical land movements associated with GIA in order to determine the climate-related rates of sea-level rise. The final reconstruction depicted a stable sea level from 100 BC to 950 AD, a rise at a rate of 0.6 mm/year from 950 AD to 1400 AD, followed by stability until the end of the 19th century. Around 1880-1920 AD the record confirmed the findings of Kemp et al. (2009b) and indicated a second increase in the rate of sea-level rise with an average rate of 2.1 mm/year.

Unpublished work by Woodson (2012) expanded on the findings of Kemp et al. (2011) by constraining the relative sea-level history for Sand Hill Point, near Tump Point, North Carolina (Figure 1). Surface foraminiferal assemblage data, along with data from previous studies (e.g., Culver and Horton, 2005; Kemp et al., 2009b), provided clear index points with respect to former sea-level elevation for the site, which extended the Kemp et al. (2011) record by 600 years. Data provided by Woodson (2012) indicated that a 2.1 m accumulation of salt-marsh peat Sand Hill Point had the potential to extend the Kemp et al. (2011) North Carolina sea-level curve.

Post-depositional lowering by compaction of samples used to reconstruct sea level can create a sea-level estimation that is too low and a rate of rise that is too great. Brain et al. (2015) used geotechnical modelling to assess the effects of compaction at Tump Point, North Carolina. The model was applied to the Tump Point core analyzed by Kemp et al. (2009b, 2011) in order to quantify the contribution of compaction to the sea-level reconstruction. Brain et al. (2015) indicated a maximum compaction contribution of 12% of reconstructed sea-level change, or 0.03 mm/year, which did not generate artificial trends. The authors considered this to be insufficient to cause significant misinterpretation of historic sea-level changes in North Carolina.

METHODS

FIELD

For sea-level studies using salt-marsh foraminifera, optimal precision is generally achieved when modern distributions are related to tidal elevations as close as possible to where they will be used as sea-level indicators (Gehrels, 1994). However, changes in foraminiferal assemblages and relationships with tidal elevation through time may necessitate the need for analogs from multiple sites within a region. Therefore, a total of 23 surface (0 – 1 cm) samples were collected along two transects to characterize the modern distribution of foraminifera at Sand Hill Point. The transects paralleled the prevailing environmental and elevation gradient inland from the edge of marsh. Sampling stations were positioned at regular vertical intervals to capture all botanical sub-environments. Thirteen samples were collected from transect 1, north of the creek, and ten samples were collected from transect 2, south of the creek (Figure 2). The samples were stored in plastic tubes containing 70% buffered alcohol for preservation and rose Bengal to stain the foraminifera alive at the time of collection (e.g., Walton, 1952; Murray and Bowser, 2000).

A Real Time Kinematic (RTK) GPS (datum NAVD88) was used to establish a temporary benchmark at Sand Hill Point and to measure the elevation of all surface and core samples relative to the North American Vertical Datum of 1988 (NAVD88). The root mean square error (RMSE) of the RTK survey was 0.012 m. Elevations were related to the local tidal datum using the National Oceanic and Atmospheric Administration's (NOAA) vertical datum transformation tool for coastal regions (VDatum) (Appendix A).

Exploratory gouge coring along transects characterized the sub-surface stratigraphy of the Sand Hill Point site. The location with the thickest sequence of salt-marsh peat was selected for

detailed analysis with the expectation that it would overlap with, and extend, the existing relative sea-level reconstruction from nearby Tump Point (Kemp et al., 2011). Cores SHP-9A and replicate core SHP-9B (Figure 2) were collected in overlapping 50 cm intervals from 80 to 290 cm depth, in order to overlap with and extend the record from Tump Point, using a Russian corer to prevent compaction and contamination during core recovery. The cores were plastic-wrapped in the field and refrigerated immediately.

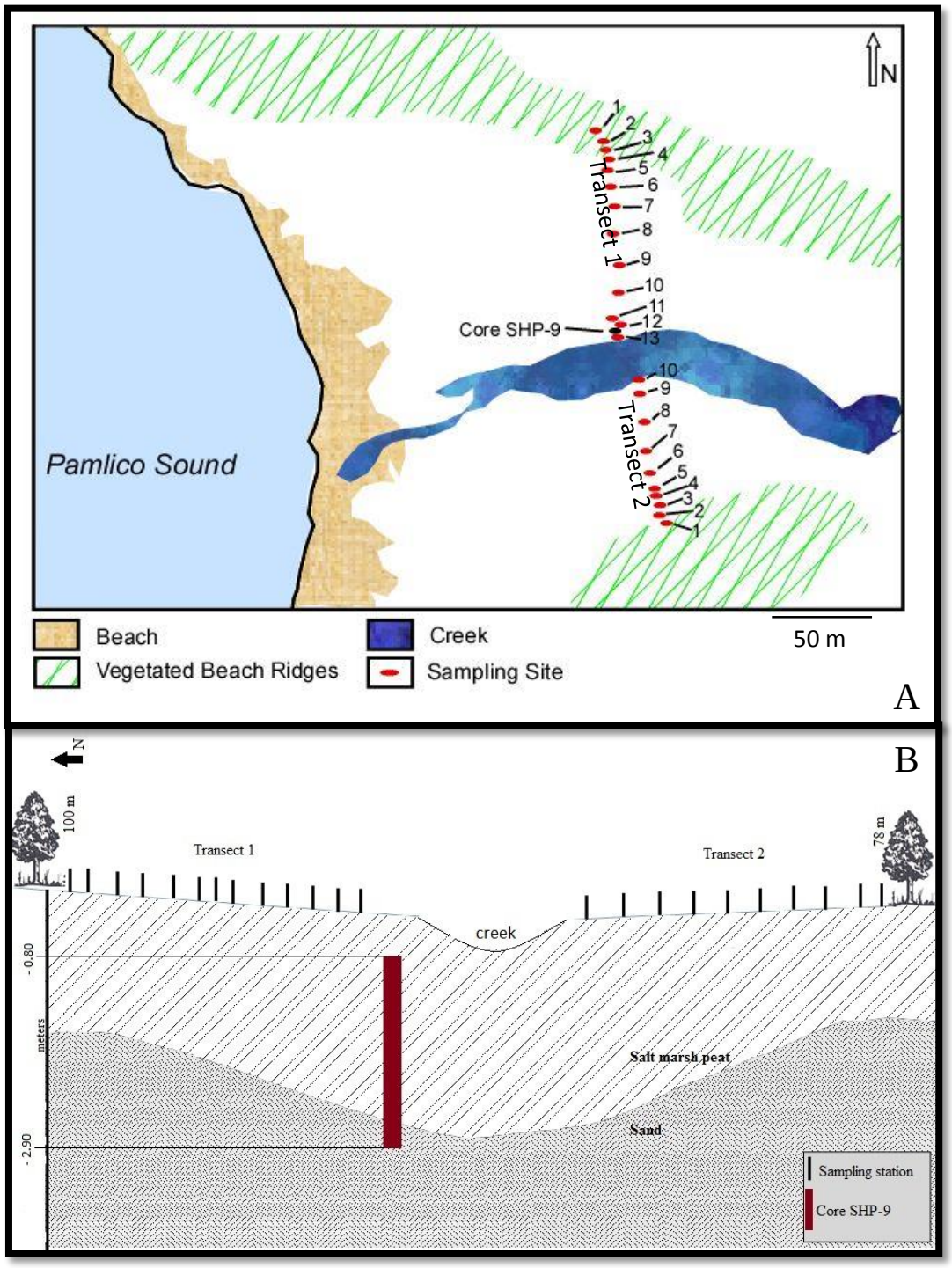

Figure 2: A: Aerial view of Sand Hill Point depicting surface samples collected from transect 1 (north of the creek) and transect 2 (south of the creek) and core SHP-9 on Cedar Island, NC. B: Cross section depicting surface sample and core SHP-9 locations. Core SHP-9 is 0.8 to 2.9 m depth. Transects 1 and 2 are depicted with furthest sample distance (meters) from the creek. Sampling station one is furthest from the creek in both transects. Individual elevation and distance data for each station can be found in Appendix A. Not to scale.

FORAMINIFERA

Preparation of both surface and core samples followed the same procedure for foraminiferal analysis. SHP9-A was sliced into contiguous 1 cm-thick samples and every other sample was processed. Each sample was washed over 710 and 63 micron sieves to isolate the foraminifera-bearing material. The <710 micron to >63 micron fraction was run through a wet splitter (Scott and Hermelin, 1993) to equally and randomly distribute the sample into eight aliquots. A known fraction of each sample was then wet-picked for at least 100 foraminiferal specimens according to standard methodology (e.g., Cronin et al., 2000; Karlson et al., 2000; Grand Pre et al., 2011). If 100 specimens were not present, the sample was picked in its entirety. Specimens were placed on a 60-square slide where they were sorted and identified to the species level. Surficial sample counts included only dead foraminifera. Only specimens in which the last chamber or all chambers were fully stained by rose Bengal were considered to be alive at the time of collection, and therefore, were excluded from the count (e.g., Horton, 1999; Horton and Edwards, 2006). A total of 16 species of salt-marsh foraminifera were identified by comparison with published literature and type specimens housed at the Smithsonian Institution, Washington, D.C. Original references for Sand Hill Point foraminiferal species are provided in Appendix D.

RADIOCARBON AGE ESTIMATES

Following Kemp et al. (2013a), SHP-9B was sliced vertically and dissected for materials considered appropriate for radiocarbon dating including *Juncus roemerianus* and *Distichlis spicata* rhizomes and stems, charcoal, and wood pieces. A total of twelve samples (Appendix E) were selected for radiocarbon dating based on the condition and location of the sample within the core to ensure best coverage possible. These samples were thoroughly cleaned under a microscope using distilled water to remove possible contaminating material including adhered

sediment and ingrowing roots, which may contain carbon older or younger than the intended sample (Kemp et al., 2013a) and influence the radiocarbon-dated ages. Samples were then dried in an oven at 40°C for five days. After drying, the samples were submitted to National Ocean Sciences Accelerator Mass Spectrometry (NOSAMS) Facility for radiocarbon dating. Samples were sent in glass vials which were also cleaned with distilled water and oven dried to avoid any possible contamination. All sample preparation and handling followed NOSAMS General Sampling Guidelines. At NOSAMS all samples underwent standard acid-base-acid pretreatment. Sample $\delta^{13}C$ was measured on an aliquot of the combusted sample and was used by NOSAMS to correct for the isotopic fraction of the sample.

AGE-DEPTH MODEL

The BChron model is an R program package which enables quick calibration of radiocarbon dates under various calibration curves and age-depth modelling, which can be used as a chronology model in late Holocene sea-level reconstructions from salt-marsh sediments (Parnell and Gehrels, 2015). BChron estimates the age of every sample in the core with an error without needing to radiocarbon date every sample. It is a flexible approach which takes the radiocarbon determinations, associated laboratory errors and depths for the samples in a core as the input, and outputs joint chronological samples summarized in an age-depth plot (Parnell et al., 2008, 2011). The BChron model was used to calibrate (Intcal13 calibration curve; Reimer et al., 2013) the Sand Hill Point radiocarbon data received from NOSAMS (Appendix E).

TRANSFER FUNCTION

Transfer functions are empirically derived equations, constructed from an understanding of the modern, observable relationship between organisms and their environment (e.g., Imbrie and Kipp, 1971; Juggins and Birks, 2012) and offer a robust methodology for sea-level reconstructions using salt-marsh deposits (e.g., Edwards and Horton, 2000; Gehrels, 2000; Edwards et al., 2004; Horton and Edwards, 2006; Massey et al., 2006; Horton and Culver, 2008; Leorri et al., 2008; Kemp et al., 2009b, 2011; Leorri et al., 2010; Juggins and Birks, 2012). This three step approach involved the development of the modern training set, development of the transfer function, and the relative sea-level reconstruction. The 23 new Sand Hill Point surficial samples were added to the regional dataset (Kemp et al., 2009a) of modern foraminiferal and elevation data points (n = 205) from 10 sites in North Carolina (Figure 1). This expanded modern training set was used to reconstruct RSL. Development of the modern training set involved establishing the elevation of modern foraminiferal assemblages relative to the tidal frame. In order to standardize the elevation of each sample, to account for vertical tidal range difference between study sites, the elevation of each sample was converted to a standardized water level index (SWLI) following standard methodology (Horton and Edwards, 2006) using the equation:

[(sample elevation – MLLW)/GT] x 100

where sample elevation is in meters above local mean sea level (LMSL) and MLLW is the mean lower low water level at Sand Hill Point. Great diurnal range (GT) (tidal range) is the difference between MLLW and mean higher high water (MHHW).

Development of the transfer function required the selection of an appropriate numerical technique to define the relationship between foraminiferal species and the tidal frame. Here, a

locally weighted-weighted average (LWWA) regression model was chosen (Batterbee et al., 2001). LWWA is a useful approach that can perform well when applied to regional data-sets (Juggins and Birks, 2012) such as that from North Carolina. This technique creates individual training sets for each fossil sample. The LWWA approach balances the precision of a small, local dataset and the wide range of modern analogs available in a larger, regional training set for reconstructing sea level (Kemp and Telford, 2015). For each fossil sample, the number of modern samples (*k*) to be included in the training set needs to be determined; generally 30-50 is considered appropriate (Juggins and Birks, 2012). For Sand Hill Point, a *k* value of 30 was justified by investigating a suite of LWWA models that were developed using values of *k* between 20 and 100 (Figure 5, panel 2). The LWWA method identifies the *k* analogs using a modern analog technique (MAT) which calculates the dissimilarity (see below) between a fossil sample and each sample in the modern training set (Kemp and Telford, 2015), and an individual transfer function is then developed for each sample. LWWA allows for the benefits of multiple methods, including MAT and weighted averaging (WA) to be utilized.

WA adopts the species abundance as the predictor and the environmental variable as the response. This method allows the value of sample where the species is highly abundant to be given more importance in calculating the average environmental value, versus a sample where the same species is less abundant or rare. This is plausible assuming that a species is more abundant at locations where environmental variables are favorable (Kemp and Telford, 2015).

MAT measures dissimilarity between fossil and modern samples using a selected metric (Kemp and Telford, 2015). Similar to the *k* value selection, the dissimilarity metric was chosen by investigating a suite of LWWA models using four dissimilarity metrics (Bray-Curtis percent dissimilarity, squared Chord distance, squared Chi-squared distance and squared Euclidean

distance). A comparison of the distance criteria showed that selection of one over the other distance metric did not affect the output (Figure 5, panel 1). The Bray-Curtis dissimilarity coefficient was chose as the distance criterion.

The transfer function was cross-validated by simulating new data from the modern training set as a mean to evaluate the transfer function model. A bootstrapping method (Juggins and Birks, 2012; Kemp and Telford, 2015) was utilized, which selects a fixed number of samples with replacement to create a new training set. The unselected samples form a test set and the procedure is repeated many times (bootstrapping = 1,000), deriving the error estimate for each fossil sample which is included in the transfer function output.

RELATIVE SEA-LEVEL RECONSTRUCTION AND REANALYSIS

The LWWA transfer function was applied to the new Sand Hill Point core and also to the existing record from nearby Tump Point to ensure that the records were directly comparable with one another. The output provided a relatable, contiguous set of paleomarsh elevations (PME) with sample-specific errors (expressed as SWLI) that was converted back to absolute tidal elevations using the modern tidal prism at each site. The sample elevation in meters above local mean sea level (m LMSL) for each sample was subtracted from the PME, according to standard methodology (e.g., Kemp et al., 2009b; 2011), in order to obtain a relative sea level value for each sample. Relative sea level (m) was plotted against age for Sand Hill Point (Figures 6 – 9) and Tump Point (Figure 7 – 9) in order to reconstruct relative sea level.

RESULTS

SAND HILL POINT CHRONOLOGY

Twelve samples from core SHP-9B were sent to the National Ocean Sciences AMS Facility (NOSAMS) for radiocarbon dating and used to establish an age-depth model (Table 1; Figure 3; Appendix E). One sample (SHP-9/166cm) was excluded from the age-depth model because the reported age was younger than any other sample and, thus, was considered to be a result of modern carbon contamination during sample preparation or during coring activities. The reported ages of the two lower-most radiocarbon samples SHP-9/246 and SHP-9/267 were significantly older than would be expected for a salt-marsh deposit at these elevations. Thus, these two samples are considered to be from a distinct unit at the base of the core (and, therefore, were excluded from the age-depth model). This is confirmed by pollen data that indicates a freshwater forested wetland (Appendix G).

The Sand Hill Point age-depth model (Figure 3) displays an approximately linear trend spanning ~1050 BC to ~1500 AD. There is a considerably large error, of up to 1000 years, below 230 cm core depth. The error is also fairly large at the top of the core. These large temporal errors are attributed to the inherent error in the BChron modelling program when extrapolating ages. No disruptions or reversals are evident in the chronology, indicating an undisturbed, relatively continuous record for sea-level reconstruction.

Table 1: Radiocarbon data used to develop the Sand Hill Point age-depth model. Calibrated age ranges were determined using OxCal 4.2 calibration software (Ramsey, 2008) with 95% confidence.

Sample Identification	Type	Process	Accession #	Age (C-14 years)	Age Error (C-14 years)	$\delta^{13}C$	2σ Age Range (AD/BC)
SHP-9/88cm	*Juncus roemerianus* stems	(OC) Organic carbon	OS-107656	625	30	-27.19	1290 AD – 1399 AD
SHP-9/98cm	*Juncus roemerianus* stems	(OC) Organic carbon	OS-107657	680	25	-26.66	1273 AD – 1388 AD
SHP-9/110cm	*Juncus roemerianus* stems	(OC) Organic carbon	OS-107658	975	30	-27.39	1013 AD – 1155 AD
SHP-9 124cm	*Juncus roemerianus* stem and root bulb	(OC) Organic carbon	OS-110628	1,180	25	-24.53	770 AD – 945 AD
SHP-9/139cm	*Juncus roemerianus* rhizome	(OC) Organic carbon	OS-107659	1,440	25	-27.55	575 AD – 652 AD
SHP-9/153cm	*Juncus roemerianus* rhizome	(OC) Organic carbon	OS-107661	1,500	20	-28.22	478 AD – 620 AD
SHP-9/166 cm	*Juncus roemerianus* stem	(OC) Organic Carbon	OS-107662	210	25	-25.97	N/A
SHP-9/177cm	*Distichlis spicata* rhizome	(OC) Organic carbon	OS-107663	1,880	25	-14.5	70 AD – 215 AD
SHP-9/206cm	Woody root bulb	(OC) Organic carbon	OS-107768	2,180	25	-28.77	359 BC – 172 BC
SHP-9 226cm	*Juncus roemerianus* stem	(OC) Organic carbon	OS-110629	2,100	25	-27.57	188 BC – 51 BC
SHP-9/246cm	Charcoal	(OC) Organic Carbon	OS-107785	3,480	25	-26.3	1885 BC – 1701 BC
SHP-9/267cm	Bed of *Scripus sp.* stems	(OC) Organic Carbon	OS-107786	5,000	35	-26.54	3943 BC – 3697 BC

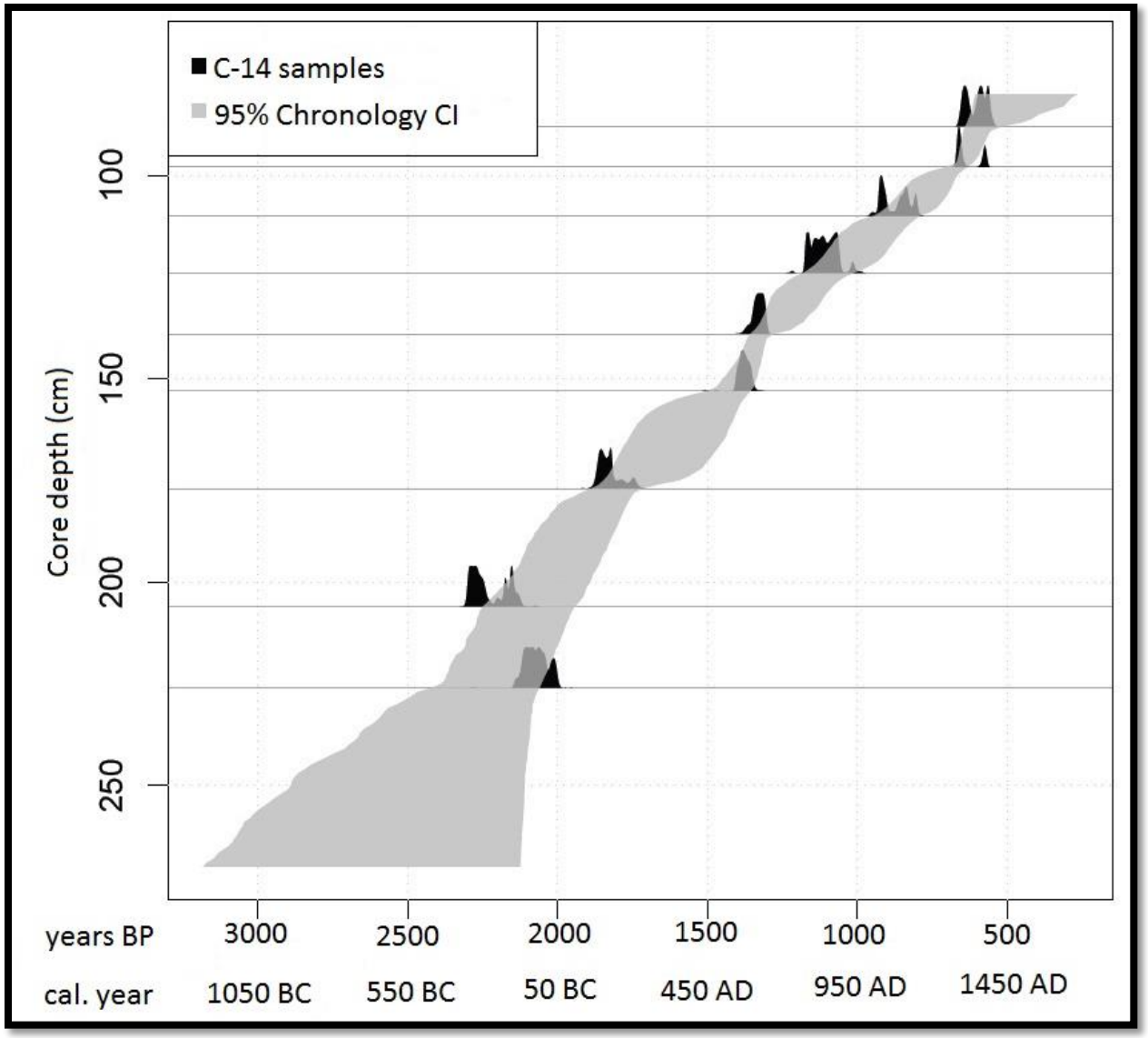

Figure 3: Sand Hill Point age-depth model created in BChron (see text for methods). The C-14 samples are represented by probability spikes (black). The gray-shaded area represents the 95% confidence interval (CI).

MODERN FORAMINIFERA

Twenty-three surface samples were collected along two transects at Sand Hill Point to characterize the modern foraminiferal distribution. Thirteen samples were collected from transect 1, north of the creek, and ten samples were collected from transect 2, south of the creek (Figure 3). Modern foraminiferal assemblages from the North Carolina regional dataset (Kemp et al., 2009a) were dominated (average ≥15% relative abundance per sample) by *Tiphotrocha comprimata, Jadammina macrescens, Ammoastuta inepta,* and *Arenoparrella mexicana.* At Sand Hill Point these species were also abundant in the surficial samples (28% average, 0 – 83% range; 17, 0 – 40; 16, 0 – 54; 3, 0 – 18, respectively). No major trends in foraminiferal species distribution over the elevation range were evident. However, *Tiphotrocha comprimata* was extremely dominant from 140 – 155 elevation (SWLI).

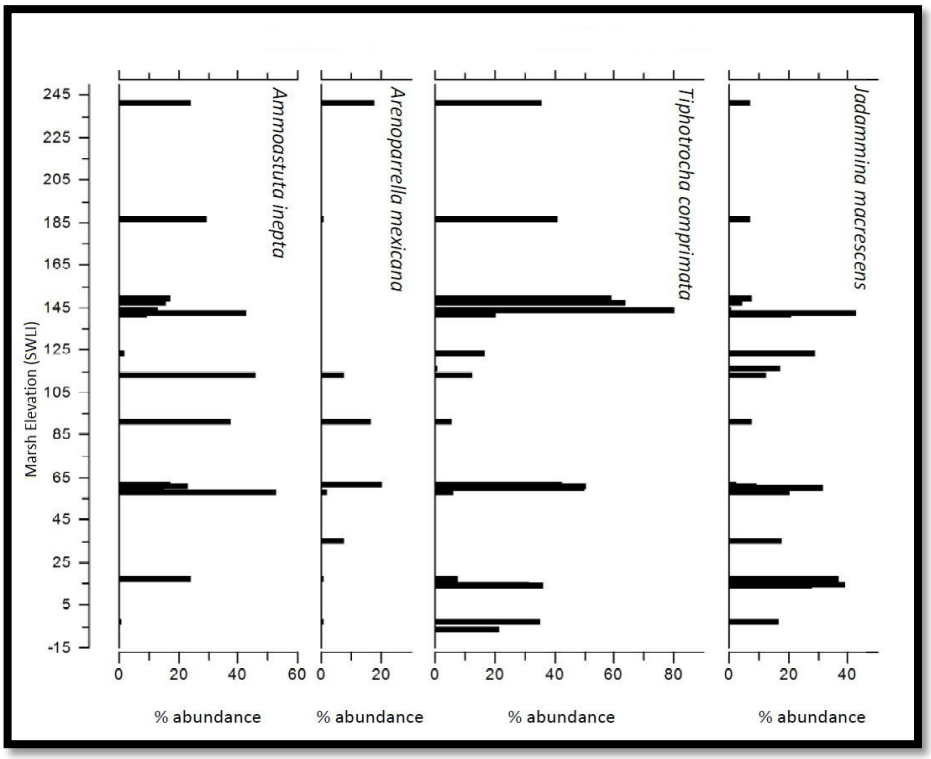

Figure 4: Relative percent abundance of the four most abundant (average ≥15% of a species in a sample) species in the regional dataset (Kemp et al., 2009a) from surficial samples at Sand Hill Point. The relative abundance is plotted against marsh elevation (SWLI).

Specimens of *Tiphotrocha comprimata* and *Jadammina macrescens* were present in all Sand Hill Point surface samples with one exception. Specimens of *Ammoastuta inepta* were present in 17 of 23 samples and specimens of *Arenoparrella mexicana* were present in only nine of 23 samples. A rare species in the regional dataset samples, *Trochamminita salsa* (21% average, 0 – 80% range) is a dominant species in Sand Hill Point surficial samples furthest inland. Secondary species at Sand Hill Point include *Trochammina inflata* (5% average, 0 – 19% range), *Miliammina fusca* (3%, 0 – 22%), and *Haplophragmoides wilberti* (2%, 0 – 19%). All other species were considered rare (<10% maximum abundance per one sample). Raw counts and relative abundance of all surface Sand Hill Point foraminiferal species are provided in Appendix C.

DOWN-CORE FORAMINIFERAL DISTRIBUTIONS AND TRANSFER FUNCTION

Trends in the relative abundance of foraminiferal species are more evident down-core (Figure 6) than in surface samples. *Tiphotrocha comprimata* (110 – 160 cm), *Jadammina macrescens* and *Ammoastuta inepta* (160 – 190 cm) dominate the middle section of the core. *Arenoparrella mexicana* dominates the lowermost and topmost sections of the core (190 – 230 cm, 80 – 110 cm respectively).

The relative abundance of *Tiphotrocha comprimata* increases with depth until 140 cm then decreases slightly and remains fairly constant (10 – 30% relative abundance) from 140 – 230 cm depth. The relative abundance of *Jadammina macrescens* increases slightly down-core, reaching its peak from 155 – 175 cm depth, followed by a decrease. Relative abundance trends of *Ammoastuta inepta* are the least evident, shifting slightly between 15% and 25% percent throughout the core. However, from 155 cm – 175 cm depth, the relative abundance surpasses 40%, matching the high abundance of *Jadammina macrescens* in this section of the core.

Relative abundance of *Arenoparrella mexicana* is highest in the topmost section of the core then decreases and remains low (<20% relative abundance) until 190 cm depth where it dominates from 190 – 230 cm depth. Foraminiferal census data for all down-core samples can be found in Appendix F.

Development of the Sand Hill Point transfer function required the choice of an appropriate model and distance metric. Four distance metric models (Bray-Curtis percent dissimilarity, Squared chord distance, Squared chi-squared distance, and Squared Euclidean distance) were run with a consistent *k* value ($k = 30$) in order to determine any disagreement of results for the different model choices. The trend of SWLI with depth is consistent between models (Figure 5). We elected to use the Bray-Curtis dissimilarity metric following Kemp et al. (2013c). The down-core percent abundance of *Tiphotrocha comprimata, Jadammina macrescens, Ammoastuta inepta,* and *Arenoparrella mexicana* are displayed alongside the SWLI with depth, for two distance metric models, Bray-Curtis percent dissimilarity and Squared chord distance, with varying sample size (*k*) values (Figure 5). Each model was run with *k* values varying from 20 to 100 in order to determine any effect of sample size on the results. There was little variability in reconstructed PME among models developed using values of *k* from 20 to 100 except from 110 – 120 cm depth and from 130 – 150 cm depth (Figure 5, gray bars). In these instances, reconstructed PME was lowest where $k = 20$ and increased to a maximum where $k = 100$. These deviations are associated with a high abundance of *Tiphotrocha comprimata* in these sections of the core. The similarity of the trends displayed between varying *k* values suggests that a value of $k=30$, as proposed by Juggins and Birks (2012), is appropriate. The transfer function performance was evaluated based on the root-mean-square error of prediction (RMSEP = 74.7). The average reconstruction error for all Sand Hill Point samples is ±0.11 m.

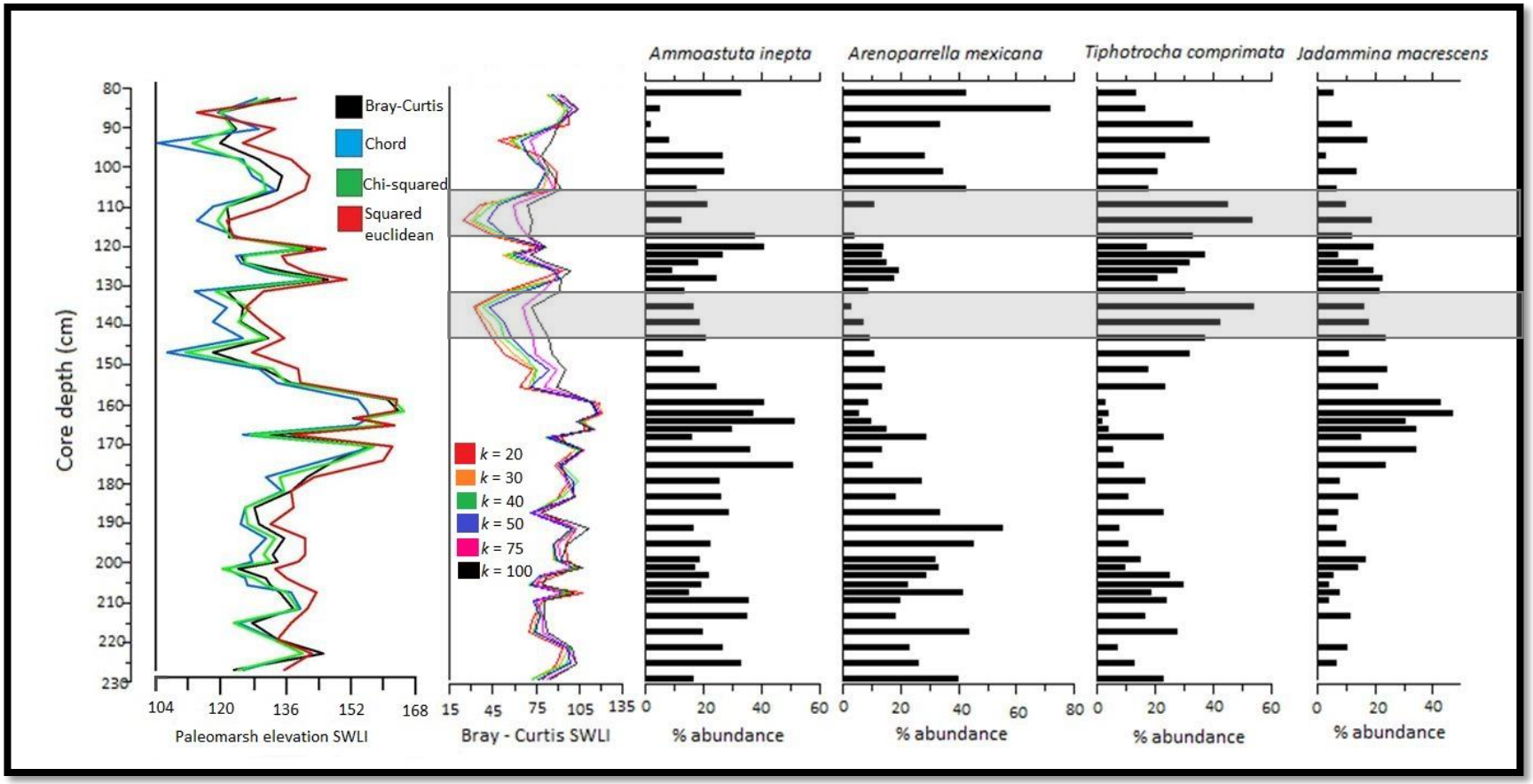

Figure 5: Down-core (SHP-9) distribution of the percent abundance per sample of the four most abundant species in the regional dataset (Kemp et al., 2009a). Panel 1 displays the four different distance metric models (Bray-Curtis percent dissimilarity, Squared chord distance, Squared chi-square distance, and Squared Euclidean distance) which were run with a consistent *k* value (*k* =30). The estimated paleomarsh elevation (SWLI) is plotted against core depth (cm) for each model. The SWLI trend with depth is consistent between models. Panel 2 displays the reconstructed standard water level index (SWLI) for the Bray-Curtis percent dissimilarity. The model was run on sample sizes (*k*) varying from 20 – 100. The gray bars highlight the slight deviations of *k* values from 110 – 120 cm depth and from 130 – 150 cm depth which is associated with high abundances of *Tiphotrocha comprimata* down-core.

RELATIVE SEA-LEVEL RECONSTRUCTION

The relative sea-level reconstruction for Sand Hill Point (Figure 6) spans ~800 BC to ~1500 AD and represents a total relative sea-level rise of 1.44 meters. All rate calculations were done using the mid-age point of each sample and without consideration of reconstruction uncertainty (vertical or temporal). The RSL record from Sand Hill Point reveals an average rate of RSL rise of 0.7 mm/year with a coefficient of determination (R^2) value of 0.98. There is an offset in the rise between ~100 AD and ~500 AD. The temporal error is largest in the earliest part of the record (800 BC to 500 BC) which is associated with the inherent error in the age-depth model (Figure 3).

Figure 6b shows the detrended RSL values (calculated by subtracting 0.7 mm/year from each data point) for the Sand Hill Point data. The linear bars (black) represent the error derived for the transfer function for each sample (red). There is no clear trend but three samples (blue) are located outside the transfer function error. These three samples are associated with the large temporal error at the top and bottom of the age-depth model suggesting that interpretation is limited by the resolution of the reconstruction and, therefore, these samples will not be discussed here.

The Sand Hill Point transfer function was also applied to the data from Tump Point (Kemp et al., 2009b, 2011) to ensure comparability. The two records agree and overlap between 600 AD and 1500 AD, a span of 800 years. The Tump Point record spans between 600 AD to and the 20th century acceleration (ca. 1915 AD; Kemp et al., 2011) with an average rate of RSL rise of 0.7mm/year with $R^2 = 0.91$. The new combined record extends from ~800 BC to 1915 AD with an average rate of RSL rise of 0.7 mm/year with $R^2 = 0.99$. The Sand Hill Point record extends the sea-level record in the Tump Point region by 1400 years (Figure 7).

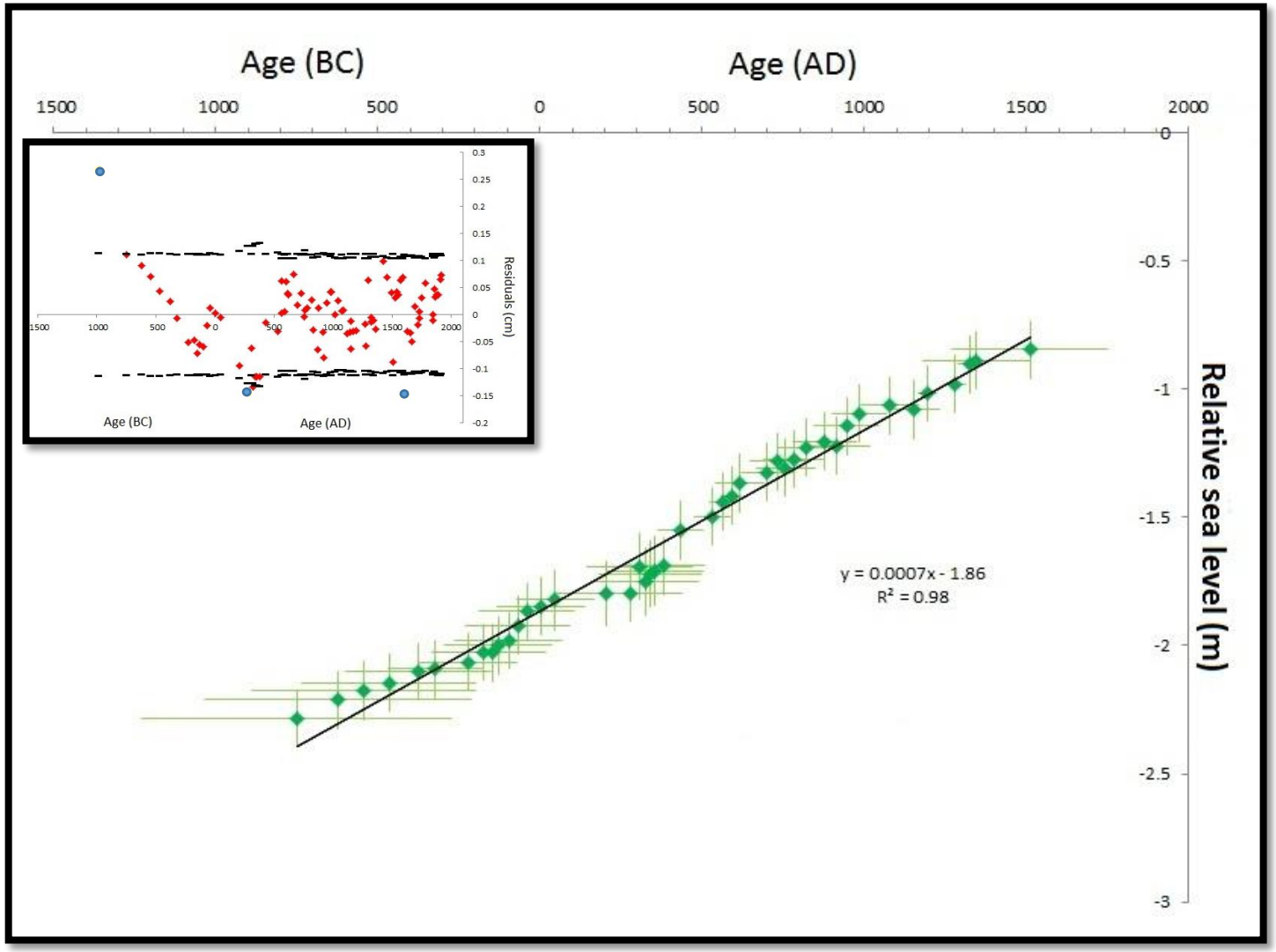

Figure 6: A: Relative sea-level record for Sand Hill Point core SHP-9. The record spans 800 BC to 1500 AD with an average rate in RSL rise of 0.7 mm/year. B: Regression analysis showing the detrended RSL values for Sand Hill Point core SHP-9 plotted against age. The error bars are shown in black, values inside error are displayed in red and three values outside of error are shown in blue.

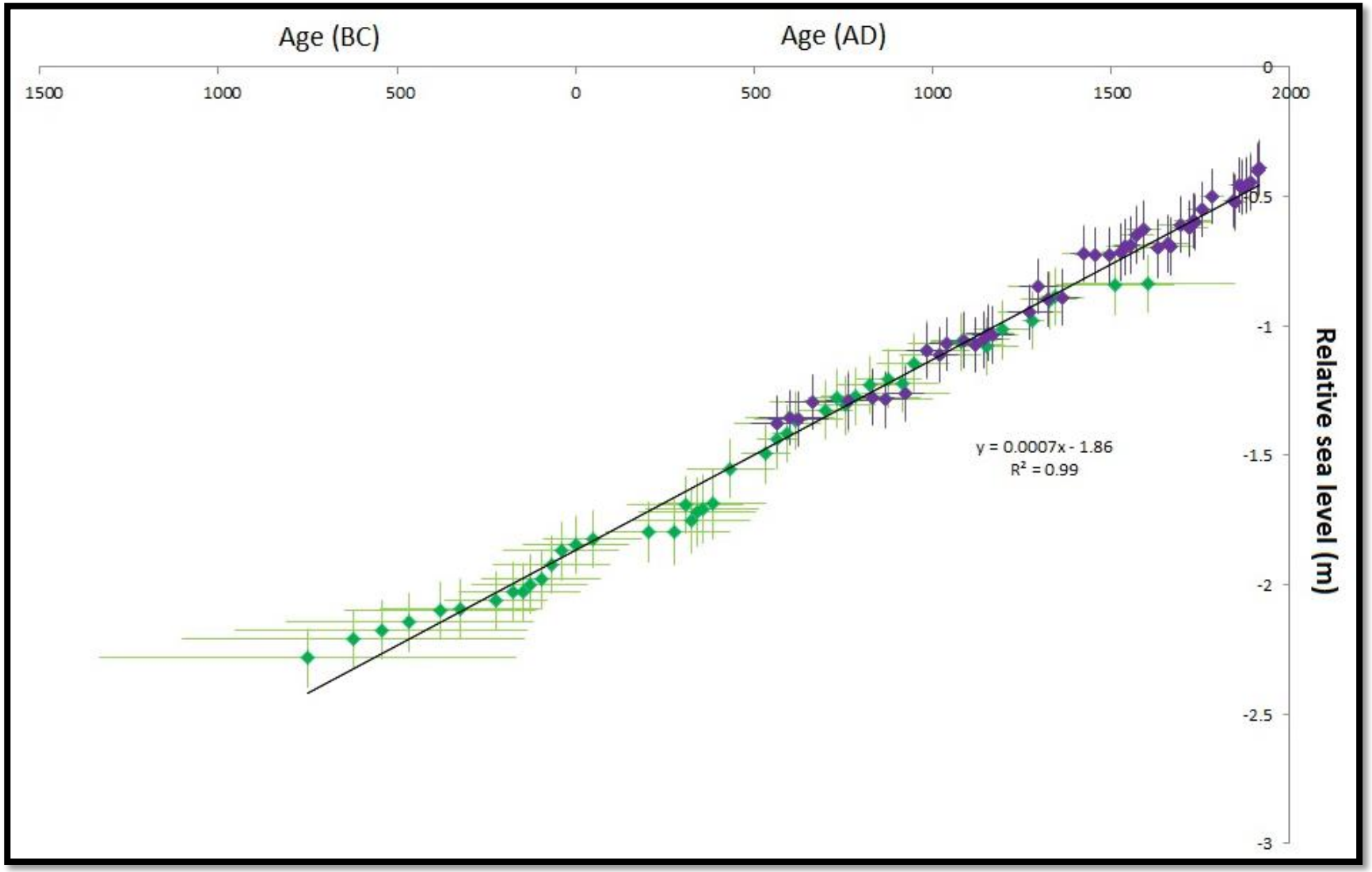

Figure 7: Relative sea-level record for Sand Hill Point (green) and Tump Point (purple) spanning 800 BC to 1915 AD with an average rate in RSL rise of 0.7 mm/year.

DISCUSSION

SAND HILL POINT FORAMINIFERA AND THE TRANSFER FUNCTION

The dissimilarity metric was chosen by investigating a suite of LWWA models using four dissimilarity metrics (Bray-Curtis percent dissimilarity, squared Chord distance, squared Chi-squared distance and squared Euclidean distance) with a consistent *k* value. A comparison of the distance criteria showed that selection of one over the other distance metric did not affect the output (Figure 5, panel 1). Following Kemp et al. (2011), the Bray-Curtis percent dissimilarity distance metric model was chosen as the final model.

Tiphotrocha comprimata is an abundant species in both the Sand Hill Point surface samples and the North Carolina regional dataset. The surface samples from Sand Hill Point reveal a possible bi-modal distribution which may be the cause of deviations in the reconstructions for the different *k* values in the Bray-Curtis percent dissimilarity distance metric model (Figure 5, panel 2). The two sections of down-core SWLI deviations in *k* correspond to sections of high relative abundance of *Tiphotrocha comprimata* (Figure 5, gray bars). It is after *k* surpasses 50 that the SWLI values begin to diverge (Figure 5, panel 2); the model begins to change its determination of where *Tiphotrocha comprimata* lives. This divergence is likely due to the fact that *Tiphotrocha comprimata* was not common in the regional dataset before the Sand Hill Point modern samples were added. The choice of $k = 30$ for the final model is justified because it is within the recommended range (Juggins and Birks, 2012) and is not associated with any significant divergence. In order to explore this, the same model was run excluding *Tiphotrocha comprimata*, however, the average SWLI value remained approximately the same (Appendix H). Therefore, all down-core foraminiferal data were included in the transfer function in order to achieve the most accurate SWLI values possible.

The choice of statistical method used can have an important impact on the performance of the transfer function (Edwards, 2007). The most common numerical methods used for sea-level research (Kemp and Telford, 2015) include Maximum Likelihood, Weighted Averaging, Weighted Averaging Partial Least Squares (WA-PLS) and Modern Analogue Technique (MAT). However, the use of the LWWA model (Batterbee et al., 2001) over other common methods allows for the benefits of multiple methods (weighted averaging and MAT) to be combined. Previous studies have shown the LWWA method to be reliable and promising (e.g., Tuovinen et al., 2010; Lamentowicz et al., 2013; Wang et al., 2013) and this method was recently used to successfully reconstruct sea level using pollen distributions (Lu et al., 2011). Here, the LWWA method was utilized for the first time using salt-marsh foraminifera. The LWWA method was ideal, choosing the 30 closest analogs for every down-core sample as defined by the Bray-Curtis dissimilarity coefficient.

The LWWA method offers an exceptionally robust technique for sea-level reconstructions in North Carolina. The original sea-level reconstruction from Tump Point, NC (Kemp et al., 2009b) used an approach similar to that used here to reconstruct the sea-level history at Sand Hill Point. Kemp et al. (2009b) utilized three separate transfer functions specifically created for three North Carolina sub-regions (Currituck, Outer Banks and Mainland). Each core sample in the study was assigned to one of the three transfer functions using measured dissimilarity. The LWWA regression model employs the same method in a more efficient way, applying an individually created transfer function to each down-core sample.

SAND HILL POINT SEA-LEVEL RECORD

The Sand Hill Point sea-level record (Figure 6) spans ~800 BC to ~1500 AD. The RSL reconstruction reveals a linear trend with an average rate of RSL rise of 0.7 mm/year. An apparent offset in the record is noted from ~100 to ~500 AD. This offset from the linear trend may be attributed to a number of factors including a major climatic event signal or a true minor oscillation in the rate of sea-level rise. Foraminifera are very poorly preserved from 176 – 143 cm core-depth. Two radiocarbon dates taken very close to these core-depths (177 cm and 139 cm, respectively) reveal ages of 206 ± 102 years AD and 591 ± 40 years AD, respectively. This poorly preserved section of the core broadly overlaps with the offset RSL section (Figure 8).

One possible explanation for the offset in the Sand Hill Point record is that it represents a true minor oscillation in the rate of sea-level rise. A slight drop in sea level could leave the marsh at Cedar Island desiccated, as evidenced by the poor foraminiferal preservation in that section of the core. The offset may also be a signature of a climatic event. It is possible that the offset in the Sand Hill Point record is a reflection of the Roman Warm Period (RWP) (Cronin et al., 2003). Timing of the RWP varies with latitude in the north Atlantic region. In a record from Scotland the RWP spans ~300 BC to 550 AD (e.g., Wang et al., 2012, 2013), which begins earlier than the offset seen in the Sand Hill Point record. A record of surface water temperature and salinity variability in the Feni Drift of the northeast Atlantic Ocean, off the coast of Ireland, relates a RWP signature spanning 180 to 560 AD (Richter et al., 2009), close in timing to the Sand Hill Point record signature (~100 AD to ~500 AD). The RWP here is associated with partly higher sea surface temperatures and higher salinities. While these records appear to be in agreement, Richter et al. (2009) noted that the onset of the RWP in the Feni Drift record appears later with respect to some other records (e.g., Desprat et al., 2003; Wang et al., 2012, 2013). One such

record from Iberia, just on the border of Spain and Portugal, utilized pollen data, and indicated a RWP signature from 250 BC – 450 AD. While the onset of the RWP appears at varying times in records across the Atlantic, the termination of the event, including in the Sand Hill Point record, is centered around 500 AD.

Records from Portugal revealed a RWP signature between 150 AD and 450 AD (Moreno et al., 2014), also in agreement with the Sand Hill Point record. The segment of the Portugal record encompassing the RWP also reveals poorly preserved tests in the foraminiferal assemblages (Moreno et al., 2014). Reconstructed precipitation and temperature from shells and otoliths in Florida, USA indicates drier summers and warmer winters during the RWP than today, the timing of which is also in agreement with archeological evidence observed from 1 – 500 AD (Wang et al., 2013). For the cooling and drying noted during the RWP in Florida, Wang et al. (2013) suggested that decreased solar radiation was likely a forcing factor. The poorly preserved foraminifera in the Sand Hill Point record during this time interval could be explained by the dryer time period. Agglutinated tests are typically more vulnerable when dry, particularly *Jadammina macrescens,* one of the most abundant species at Sand Hill Point that is prone to the collapse of chambers during burial (Kemp, 2009).

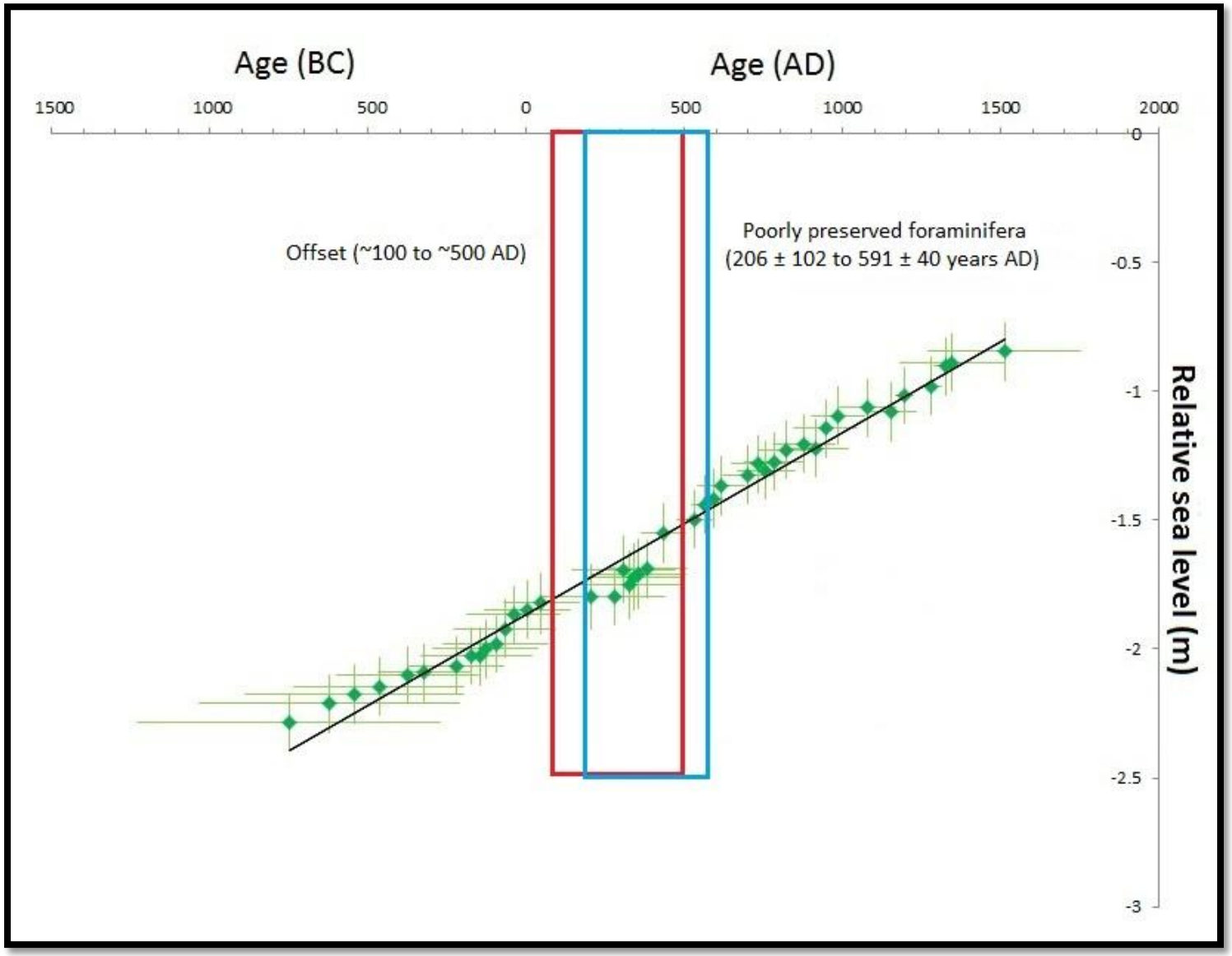

Figure 8: Relative sea-level record for Sand Hill Point highlighting the section of offset (red) and section of poorly preserved down-core foraminifera (blue).

NORTH CAROLINA LATE HOLOCENE SEA-LEVEL RECORD

The combination of data from multiple cores can improve the resulting chronology (e.g., Horton and Edwards, 2006; Edwards, 2007). The Sand Hill Point record agrees well ($R^2 = 0.99$) with the record from nearby Tump Point (Figure 7). The combined record is also in general agreement with other North Carolina sea-level studies (e.g., Horton et al., 2009; Kemp et al., 2011; Kopp et al., 2014).

Kemp et al. (2011) reconstructed sea level from Tump Point and Sand Point, North Carolina (Figure 1) since ~100 BC. The analysis suggested that, for North Carolina, sea level was stable from 100 BC – 950 AD, rose at an average rate of 0.6 mm/year (0.4 to 0.8 mm/year) from 950 AD – 1400 AD, was stable again from 1400 AD – ~1900 AD, then rose at an accelerated rate of 2.1 mm/year into the twentieth century. The new combined record from Sand Hill Point and Tump Point is similar to the Kemp et al. (2011) record between 950 AD and 1400 AD, agreeing within error. The stability revealed from 100 BC – 950 AD can be seen also in the new Tump Point record. However, although it lies exactly atop the Sand Hill Point record (Figure 7), the rate of relative sea-level rise from 100 BC – 950 AD at Tump Point is, within error, possibly representative of a slight increase in the rate of sea level rise.

Sea-level change at Sand Point in Croatan Sound, North Carolina (Figure 1), displayed an average rate of 1.11 ±0.03 mm/year between 1800 BC and 0 BC (Kopp et al., 2014). This higher average rate of sea-level rise, as compared to Tump Point, may be explained by the general trend of relative sea-level along the U.S. Atlantic coast. Rates of relative sea-level rise are greatest in the mid-Atlantic region and decrease gradually southward (Kemp et al., 2014) as a result of variations in subsidence rates related to glacio-isostatic processes (Kemp et al., 2014).

Recent work in the APES (Zaremba, 2014) estimated a sea-level curve spanning the last 7000 years by applying a correction for local subsidence to a previously developed eustatic curve. The sea-level curve was calibrated using sea-level index and limiting points (Horton et al., 2009) and, along with the local sea-level curve from Kemp et al. (2011), estimated an average, relatively stable rate of sea level rise of 1.0 ± 0.3 mm/year for Pamlico Sound from 3500 to 1200 cal BP, encompassing much of the Sand Hill Point record.

REGIONAL COMPARISON

The new combined sea-level record from Sand Hill Point and Tump Point reveals an average rate of sea-level rise of 0.7 mm/year from 800 BC to 1915 AD. Holocene rates of sea-level rise are well documented in eastern United States (e.g., van de Plassche, 1991; Gehrels, 1999; Edwards et al., 2004; Engelhart et al., 2009, 2011a; Engelhart and Horton, 2012; Kemp et al., 2013b, 2014; Kopp et al., 2014; Kemp et al., 2015) and the average rate of rise varies along the coastline (Figure 9). A database of 473 Holocene sea level index points (Engelhart et al., 2011a) spanning the eastern United States coastline from Maine to South Carolina has been established in order to assess spatial variability in rates of relative sea-level rise. While the database spans the entire Holocene, the authors suggested that the spatial variation is likely related to the collapsing Laurentide Ice Sheet forebulge (Figure 9). Temporally, the record indicates that along the US Atlantic coast, rates of relative sea-level rise were highest during the early Holocene and have decreased over time due. This decrease is suggested to be in response to the continued response to glacial isostatic adjustment (GIA) (Engelhart et al., 2011a, 2011b) associated with the relaxation response of the Earth's mantle and the reduction of meltwater input (Engelhart and Horton, 2012), with the highest rates of rise occurring in New Jersey and Delaware.

Expanding on the work of Engelhart et al. (2011a), Engelhart and Horton (2012) presented a full database, including 164 new index points, of relative sea level estimates for the Holocene along the US Atlantic coast, indicating an average rate of relative sea-level rise of ~0.8 mm/year from 4000 BP to 1900 AD in the northeastern Atlantic region (Maine, Massachusetts, Connecticut; Figure 9). Average rates of sea-level rise calculated using a transfer function on foraminiferal assemblages from salt-marsh peat in Machiasport, Maine revealed an average rate of 0.75 mm/year between 6000 and 1500 cal yr BP (Gehrels, 1999). This timing corresponds to the later part of the Sand Hill Point record to 450 AD. Hundreds of cores from Hammock River marsh in Connecticut were analyzed for stratigraphic boundaries in order to demonstrate times of low and high marsh expansion relative to sea-level fluctuations. The record revealed five separate fluctuations in sea level during the last 2200 years with an average rate of rise of about 0.8 mm/year (van de Plassche, 1991).

An average rate of ~1.4 mm/year is documented in the mid-Atlantic region (New York, New Jersey, Delaware, and Virginia, Figure 9) spanning 4000 BP – 1900 AD (Engelhart and Horton, 2012). The New Jersey record (Kemp et al., 2013b) in particular reveals four major periods of different sea-level trends including a general sea-level fall of 0.11 mm/year from 500 BC – 250 AD, a sea-level rise of 0.62 mm/year from 250 AD – 733 AD, a general sea-level fall of 0.12 mm/year from 733 AD – 1850 AD, and the onset of accelerated sea-level rise at a rate of 3.1 mm/year since 1850 AD. The mid-Atlantic region lies just north of Sand Hill Point and Tump Point, where the highest rates of sea-level rise have been documented (Engelhart and Horton, 2012).

Average rates of sea-level rise of ~0.5 – 1.0 mm/year are seen from 4000 BP to 1900 AD for the southeastern Atlantic region encompassing North Carolina and South Carolina (Figure 9).

Engelhart and Horton (2012) suggested that the lower rates in the southeastern Atlantic region are associated with lower rates of GIA-related subsidence compared to more northern states (mid-Atlantic and northeastern regions). While a shorter record, recent work in Florida (Kemp et al., 2014; Figure 9) agreed with this pattern, estimating the average rate of relative sea level rise of ~0.4 mm/year from 700 BC to 1800 AD.

The calculated average rate of relative sea-level rise at Sand Hill Point (0.7 mm/year) fits within previously documented rates of relative sea-level rise for the APES (0.5 – 1.0 mm/year; e.g., Engelhart and Horton, 2012; Zaremba 2014). Summary works assessing the spatial variability of relative sea-level rise along the US Atlantic coast (e.g., Engelhart et al., 2009, 2011a; Engelhart and Horton, 2012; Kemp et al., 2014) suggested that deglaciation of the Laurentide Ice Sheet (Figure 9) and subsidence of the glacial forebulge may be a factor driving the spatial variability, from 0.6 – 1.8 mm/year, with a decreasing rate from the north to the south, during the late Holocene. While there is strong evidence for the Laurentide Ice Sheet deglaciation being a major cause driving the spatial variability, other processes are likely also contributing to the trend. Recent studies suggested that local tectonism may be contributing as much as 0.24 ± 0.15 mm/year to sea-level rise in southern North Carolina (van de Plassche et al., 2014). Further, processes including thermal expansion, ocean dynamics, mountain glacier and ice cap loss, and groundwater extraction may also aid in increasing the rate of future relative sea-level rise along the US mid-Atlantic coast (Miller et al., 2013).

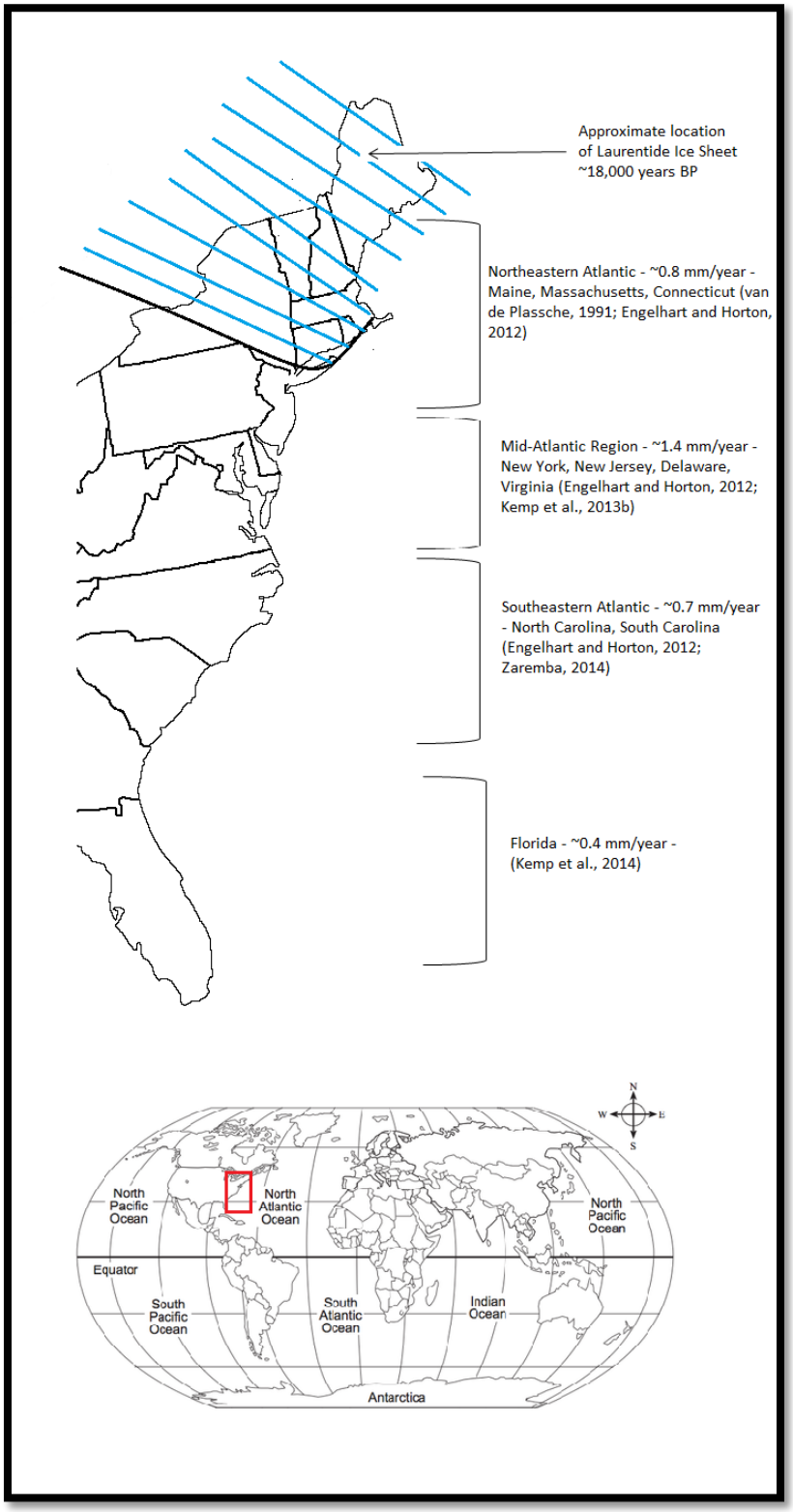

Figure 9: US Atlantic coast depicting average rate of sea-level rise for the northeastern Atlantic, mid-Atlantic, southeastern Atlantic, and Florida regions during the late Holocene with respective references and approximate location of the Laurentide Ice Sheet ~18,000 years ago (blue).

CONCLUSIONS

Surface and down-core assemblages of agglutinated salt-marsh foraminifera from Sand Hill Point, Cedar Island, North Carolina were added to the North Carolina regional dataset (Kemp et al., 2011). The new regional dataset was used with a locally weighted-weighted average (LWWA) regression model to develop a new transfer function for reconstructing late Holocene sea-level rise for the southern Albemarle-Pamlico Estuarine System (APES) in North Carolina. The new transfer function was applied to both Sand Hill Point and nearby Tump Point on Cedar Island. A relative sea-level reconstruction for Sand Hill Point was produced, extending the record from Tump Point by 1400 years. The new continuous sea-level record for the southern APES in North Carolina spans 1500 BC – 1915 AD and reveals a stable trend of relative sea-level rise at an average rate of 0.7 mm/year. This rate agrees with previously documented rates of relative sea-level rise along the US Atlantic coast.

REFERENCES

Andersen, H.V., 1953. Two new species of *Haplophragmoides* from the Louisiana coast: Contributions from the Cushman Foundation, v. 4, p. 21 – 22.

Batterbee, R.W., Juggins, S., Gasse, F., Anderson, N.J., Bennion, H., Cameron, N.G., Ryves, D.B., Pailles, DC., Chalie, F., and Telford, R., 2001. European Diatom Database (EDDI). An Information System for Palaeoenvironmental Reconstruction. ECRC Research Report, p. 81 – 91.

Brady, G.S. and Robertson, D., 1870. The ostracoda and foraminifera of tidal rivers with an analysis and description of foraminifera. Annals and Magazine of Natural History, v. 6, p. 273 – 309.

Brain, M.J., Kemp, A.C., Horton, B.P., Culver, S.J., Parnell, A.C., and Cahill, N., 2015. Quantifying the contribution of sediment compaction to late Holocene salt-marsh sea-level reconstructions, North Carolina, USA. Quaternary Research, v. 83, p. 41 – 51.

Callard, S.L., Gehrels, W.R., Morrison, B.V., and Grenfell, H.R., 2011. Suitability of salt-marsh foraminifera as proxy indicators of sea level in Tasmania. Marine Micropaleontology, v. 79, p. 121 – 131.

Christian, R.R., Bryant, W.L., and Brinson, M.M., 1990. *Juncus roemerianus* production and decomposition along gradients of salinity and hydroperiod. Marine Ecology Progress Series, v. 68, p. 137 – 145.

Church, J.A. and White, N.J., 2006. A 20th century acceleration in global sea-level rise. Geophysical Research Letters, v. 33, p. 1 – 4.

Cronin, T.M., Dwyer, G.S., Kamiya, T., Schwede, S., and Willard, D.A., 2003. Medieval Warm Period, Little Ice Age and 20th century temperature variability from Chesapeake Bay. Global and Planetary Change, v. 26, p. 17 – 29.

Cronin, T., Willard, D., Karlson, A., Ishman, S., Verardo, S., McGeehin, J., Kerhin, R., Holmes, C., Colman, S., and Zimmerman, A., 2000. Climatic variability in the eastern United States over the past millennium from Chesapeake Bay sediments. Geology, v. 28, p. 3 – 6.

Cushman, J.A. and Bronnimann, P., 1948a. Some new genera and species of Foraminifera from brackish water of Trinidad. Contributions from the Cushman Laboratory for Foraminiferal Research, v. 24, p. 15 – 21.

Cushman, J.A. and Bronnimann, P., 1948b. Additional new species of arenaceous Foraminifera from the shallow waters of Trinidad. Contributions from the Cushman Laboratory for Foraminiferal Research, v. 24, p. 37 – 42.

Cushman, J.A. and McCulloch, I., 1939. A report on some arenaceous Foraminifera: Alan Hancock Pacific Expidition, v. 6, p. 1 – 113.

Culver, S.J. and Horton, B.P., 2005. Infaunal marsh Foraminifera from the Outer Banks, North Carolina, U.S.A. Journal of Foraminiferal Research, v. 35, p. 148 – 170.

Desprat, S., Goni, M.F.S. and Loutre, M-F., 2003. Revealing climatic variability of the last three millennia in northwestern Iberia using pollen influx data. Earth and Planetary Science Letters, v. 213, p. 63 – 78.

Edwards, R., 2007. Sea levels: resolution and uncertainty. Progress in Physical Geography, v. 21, p. 621 – 632.

Edwards, R.J. and Horton, B.P., 2000. Reconstructing relative sea-level change using UK salt-marsh foraminifera. Marine Geology, v. 169, p. 41 – 56.

Edwards, R.J., van de Plassche, O., Gehrels, W.R., and Wright, A.J., 2004. Marine Micropaleontology, v. 51, p. 239 – 255.

Engelhart, S.E. and Horton, B.P., 2012. Holocene sea level database for the Atlantic coast of the United States. Quaternary Science Reviews, v. 54, p. 12 – 25.

Engelhart, S.E., Horton, B.P., Douglas, B.C., Peltier, W.R. and Tornqvist, T.E., 2009. Spatial variability of late Holocene and 20th century sea-level rise along the Atlantic coat of the United States. Geology, v. 37, p. 1115 – 1118.

Engelhart, S.E., Horton, B.P., and Kemp, A.C., 2011a. Holocene sea level changes along the United States' Atlantic Coast. Oceanography, v. 24, p. 70 – 79.

Engelhart, S.E., Peltier, W.R., and Horton, B.P., 2011b. Holocene relative sea-level changes and glacial isostatic adjustment of the U.S. Atlantic coast. Geology, v. 39, p. 751 – 754.

Gehrels, W.R., 1994. Determining relative sea-level change from salt-marsh Foraminifera and plant zones on the coast of Maine, U.S.A. Journal of Coastal Research, v. 10, p. 990 – 1009.

Gehrels, W.R., 1999. Middle and late Holocene sea-level changes in eastern Maine reconstructed from foraminiferal saltmarsh stratigraphy and AMS ^{14}C dates on basal peat. Quaternary Research, v. 52, p. 350 – 359.

Gehrels, W.R., 2000. Using foraminiferal transfer functions to produce high-resolution sea-level records from salt-marsh deposits, Maine, USA. The Holocene, v. 10, p. 367 – 376.

Gehrels, W.R., 2007. Sea level studies: microfossil reconstructions. In: Elias, S.A. (ed.) Encyclopedia of Quaternary Science, Elsevier, Amsterdam, p. 3015 – 3024.

Gehrels, W.R., Kirby, J.R., Prokoph, A., Newnham, R.M., Achterberg, E.P., Evans, H., Black, S., and Scott, D.B., 2005. Onset of recent rapid sea-level rise in the western Atlantic Ocean. Quaternary Science Reviews, v. 24, p. 2083 – 2100.

Gehrels, W.R. and Newman, S.W.G., 2004. Salt-marsh foraminifera in Ho Bugt, western Denmark, and their use as sea-level indicators. Geografisk Tidsskrift-Danish Journal of Geography, v. 104, p. 97 – 106.

Grand Pre, C., Culver, S.J., Mallinson, D.J., Farrell, K.M., Corbett, D.R., Horton, B.P., Hillier, C., Riggs, S.R., Snyder, S.W., and Buzas, M.A., 2011. Rapid Holocene coastal change revealed by high-resolution micropaleontological analysis, Pamlico Sound, North Carolina, USA. Quaternary Research, v. 76, p. 319 – 334.

Guilbault, J., Clague, J.J., and Lapointe, M., 1996. Foraminieral evidence for the amount of coseismic subsidence during a late Holocene earthquake on Vancouver Island, West Coast of Canada. Quaternary Science Reviews, v. 15, p. 913 – 937.

Gunnell, J.R., Rodriguez, A.B., and McKee, B.A., 2013. How a marsh is built from the bottom up. Geology, v. 41, p. 859 – 862.

Heron-Allen, E., and Earland, A., 1930. The foraminifera of the Plymouth District, II. Journal of the Royal Microscopical Society, v. 50, p. 161 – 199.

Horton, B.P., 1999. The contemporary distribution of intertidal foraminifera of Cowpen Marsh, Tees Estuary, UK: implications for studies of Holocene sea-level changes. Palaeogeography, Palaeoclimatology, Palaeoecology, Special Issue, v. 149, p. 127 – 149.

Horton, B.P. and Culver, S.J., 2008. Modern intertidal foraminifera of the Outer Banks, North Carolina, U.S.A., and their applicability for sea-level studies. Journal of Coastal Research, v. 24, p. 1110 – 1125.

Horton, B.P. and Edwards, R.J., 2006. Quantifying Holocene sea-level change using intertidal foraminifera: lessons from the British Isles. Cushman Foundation for Foraminiferal Research, Special Publication no. 40, p. 1 – 97.

Horton, B.P., Edwards, R.J., and Lloyd, J.M., 1999a. UK intertidal foraminiferal distributions: implications for sea-level studies. Marine Micropaleontology, v. 36, p. 205 – 223.

Horton, B.P., Edwards, R.J., Lloyd, J.M., 1999b. A foraminiferal-based transfer function: implications for sea-level studies. Journal of Foraminiferal Research, v. 29, p. 117 – 129.

Horton, B.P., Peltier, W.R., Culver, S.J., Drummond, R., Engelhart, S.E., Kemp, A.C., Mallinson, D., Thieler, E.R., Riggs, S.R., Ames, D.V., and Thomson, K.H., 2009. Holocene sea-level changes along the North Carolina Coastline and their implications for glacial isostatic adjustment models. Quaternary Science Reviews, v. 28, p. 1725 – 1736.

Imbrie, J. and Kipp, N.G., 1971. A new micropaleontological method for quantitative paleoclimatology: application to a Late Pleistocene Caribbean core. In: Turekian, K. (ed.) The Late Cenozoic Glacial Ages, Yale University Press, New Haven, p. 71 – 81.

Juggins, S. and Birks, H. J. B., 2012. Quantitative environmental reconstructions from biological data. In: Last, W.M. and Smol, J.P. (eds.) Tracking Environmental Change Using Lake Sediments, Developments in Paleoenvironmental Research, v. 5, p. 431 – 494.

Karlson, A.W., Cronin, T.M., Ishman, S.E., Willard, D.A., Holmes, C.W., and Marot, M., 2000. Historical trends in Chesapeake Bay dissolved oxygen based on benthic foraminifera from sediment cores. Estuaries, v. 23, p. 488 – 508.

Kemp, A.C., 2009. High Resolution Studies of late Holocene Relative Sea-Level Change (North Carolina, USA). Dissertation, University of Pennsylvania, p. 1 – 361.

Kemp, A.C., Bernhardt, C.E., Horton, B.P., Kopp, R.E., Vane, C.H., Peltier, W.R., Hawkes, A.D., Donnelly, J.P., Parnell, A.C., and Cahill, N., 2015. Late Holocene sea- and land-level change on the U.S. southeastern Atlantic coast. Marine Geology, v. 357, p. 90 – 100.

Kemp, A.C., Horton, B.P., and Culver, S.J., 2009a. Distribution of modern salt-marsh foraminifera in the Albemarle–Pamlico estuarine system of North Carolina, USA: implications for sea-level research. Marine Micropaleontology, v. 72, p. 222 – 238.

Kemp, A.C., Horton, B.P., Culver, S.J., Corbett, D.R., van de Plassche, O., Gehrels, W.R., Douglas, B.C., and Parnell, A.C., 2009b. Timing and magnitude of recent accelerated sea-level rise (North Carolina, United States). Geology, v. 37, p. 1035 – 1038.

Kemp, A.C., Horton, B.P., Donnelly, J.P., Mann, M.E., Vermeer, M., and Rahmstorf, S., 2011. Climate related sea-level variations over the past two millennia. PNAS, v. 108, p. 11017 – 11022.

Kemp, A.C., Nelson, A.R., and Horton, B.P., 2013a. Radiocarbon Dating of Plant Macrofossils from Tidal-Marsh Sediment. In: Shroder, J.F., Switzer, A.D. and Kennedy, D.M. (eds.) Treatise on Geomorphology, Elsevier, San Diego, p. 370 – 388.

Kemp, A.C., Horton, B.P., Vane, C.H., Bernhardt, C.E., Corbett, D.R., Engelhart, S.E., Anisfeld, S.C., Parnell, A.C., and Cahill, N., 2013b. Sea-level change during the last 2500 years in New Jersey, USA. Quaternary Science Reviews, v. 81, p. 90 – 104.

Kemp, A.C. and Telford, R.J., 2015. Transfer Functions. In: Shennan, I., Long, A.J., Horton, B.P. (eds.), Handbook of Sea Level Research, John Wiley & Sons, West Sussex, p. 470 – 499.

Kopp, R.E., Horton, B.P., Kemp, A.C., and Tebaldi, C., 2014. Past and future sea-level rise along the coast of North Carolina, United States. *arXiv preprint arXiv:1410.8369* p. 1 – 12.

Kornfeld, M.M., 1931. Recent littoral Foraminifera from Texas and Louisiana: Contributions from the Department of Geology, Stanford University, v. 1, p. 77 – 101.

Lamentowicz, M., Lamentowicz, L., and Payne, R.J., 2013. Towards quantitative reconstruction of peatland nutrient status from fens. The Holocene, v. 23, p. 1661 – 1665.

Leorri, E., Horton, B.P., and Cearreta, A., 2008. Development of a foraminifera-based transfer function in the Basque marshes, N. Spain: implications for sea-level studies in the Bay of Biscay. Marine Geology, v. 251, p. 60 – 74.

Leorri, E., Gehrels, W.R., Horton, B.P., Fatela, F., and Cearreta, A., 2010. Distribution of foraminifera in salt-marshes along the Atlantic coast of SW Europe: tools to reconstruct past sea-level variations. Quaternary International, v. 221, p. 104 – 115.

Lu, H., Wu, N., Liu, K., Zhu, L., Yang, X., Yao, T., Wang, L., Liu, X., Shen, C., Li, X., Tong, G., and Jiang, H., 2011. Modern pollen distributions in Qinghai-Tibetan Plateau and the development of transfer functions for reconstructing Holocene environmental changes. Quaternary Science Reviews, v. 30, p. 947 – 966.

Massey, A.C., Gehrels, W.R., Charman, D.J., and White, S.V., 2006. An intertidal foraminifera-based transfer function for reconstructing Holocene sea-level change in southwest England. Journal of Foraminiferal Research, v. 36, p. 215 – 232.

Miller, K.G., Kopp, R.E., Horton, B.P., Browning, J.V., and Kemp, A.C., 2013. A geological perspective on sea-level rise and its impacts along the U.S. mid-Atlantic coast. Earth's Future, v. 1, p. 3 – 48.

Montagu, G., 1808. Testacea Britannica, or, natural history of British shells. Exeter, England, p. 1 – 334.

Moreno, J., Fatela, F., Leorri, E. De la Rose, J.M., Pereira, I., Araujo, M.F., Freitas, M.C., Corbett, D.R., and Medeiros, A., 2014. Marsh benthic Foraminifera response to estuarine hydrological balance driven by climate variability over the last 2000 years (Minho estuary, NW Portugal). Quaternary Research, v. 82, p. 318 – 330.

Murray, J.W., 1968.The living Foraminifera of Christchurch Harbour, England. Micropaleontology, v. 14, p. 83-96.

Murray, J.W. and Bowser, S.S., 2000. Mortality, protoplasm decay rate, and reliability of staining techniques to recognize 'living' foraminifera: a review. Journal of Foraminiferal Research, v. 30, p. 66 – 70.

Parnell, A.C., Buck, C.E., and Doan, T.K., 2011. A review of statistical chronology models for high-resolution, proxy-based Holocene palaeoenvironmental reconstruction. Quaternary Science Reviews, v. 30, p. 2948 – 2960.

Parnell, A.C. and Gehrels, W.R., 2015. Using chronological models in late Holocene sea-level reconstructions from saltmarsh sediments. In: Shennan, I., Long, A.J., Horton, B.P. (eds.), Handbook of Sea Level Research, John Wiley & Sons, West Sussex, p. 500 – 514.

Parnell, A.C., Haslett, J., Allen, J.R.M., Buck, C.E., and Huntley, B., 2008. A flexible approach to assessing synchroneity of past events using Bayesian reconstructions of sedimentation history. Quaternary Science Reviews, v. 27, p. 1872 – 1885.

Phleger, F.B, 1965. Patterns of marsh foraminifera, Galveston Bay, Texas. Limnology and Oceanography, v. 10, p. 169 – 184.

Phleger, F.B, 1970. Foraminiferal populations and marine marsh processes. Limnology and Oceanography, v. 15, p. 522 – 534.

Ramsey, C.B., 2008. Deposition models for chronological records. Quaternary Science Reviews, v. 27, p. 42 – 60.

Reimer, P.J., Bard, E., Bayliss, A., Beck, J.W., Blackwell, P.G., Bronk, R.C., Buck, C.E., Cheng, H., Edwards, R.L., Friedrich, M., Grootes, P.M., Guilderson, T.P., Haflidason, H., Hajdas, I., Hatté, C., Heaton, T.J., Hoffmann, D.L., Hogg, A.G., Hughen, K.A., Kaiser, K.F., Kromer, B., Manning, S.W., Niu, M., Reimer, R.W., Richards, D.A., Scott, E.M., Southon, J.R., Staff, R.A., Turney, C.S.M., and van der Plicht, J., 2013. IntCal13 and Marine13 radiocarbon age calibration curves 0–50,000 years cal BP. Radiocarbon 55, 1869 – 1887.

Richter, T.O., Peeters, F.J.C. and van Weering, T.C.E., 2009. Late Holocene (0 – 2.4 ka BP) surface water temperature and salinity variability, Feni Drift, NE Atlantic Ocean. Quaternary Science Reviews, v. 28, p. 1941 – 1955.

Riggs, S., Ames, D., Culver, S.J., and Mallinson, D., 2008. The Battle for North Carolina's Coast: Evolutionary History, Present Crisis, and Vision for the Future, University of North Carolina Press: Chapel Hill, p. 1 – 142.

Roelofs, E.W. and Bumpus, D.F., 1953. The hydrography of Pamlico Sound. Bulletin of Marine Science, v. 3, p. 181 – 205.

Saunders, J.B., 1957. Trochamminidea and certain Lituolidae (foraminifera) from the recent brackish-water sediments of Trinidad, British West Indies. Smithsonian Miscellaneous Collections, v. 134, p. 1 – 16.

Saunders, J.B., 1958. Trochamminidea and certain Lituolidae (foraminifera) from the recent brackish-water sediments of Trinidad, British West Indies. Micropaleontology, v. 4, p. 86 – 87.

Scott, D.B. and Hermelin, J.O.R., 1993. A device for precision splitting of micropaleontological samples in liquid suspension. Journal of Paleontology, v. 67, p. 151 – 154.

Scott, D.B., 1976. Quantitative studies of marsh foraminiferal patterns in southern California and their application to Holocene stratigraphic problems: First International Symposium on Benthonic Foraminifera of Continental Margins, Part A, Ecology and Biology, Maritime Sediments. Special Publication, no. 1, p. 153 – 170.

Scott, D.B. and Medioli, F.S., 1978. Vertical zonation of marsh foraminifera as accurate indicators of former sea levels. Nature, v. 272, p. 528 – 531.

Scott, D.B. and Medioli, F.S., 1980, Quantitative studies of marsh foraminiferal distributions in Nova Scotia: implications for sea-level studies. Cushman Foundation for Foraminiferal Research, Special Publication no. 17, p. 1 – 58.

Shennan, I., 1982. Interpretation of Flandrian sea-level data from Fenland, England. Proceedings of the Geologists' Association, v. 93, p. 53 – 63.

Shennan, I. and Woodworth, P.L., 1992. A comparison of late Holocene and twentieth-century sea-level trends from the UK and the North Sea region. Geophysical Journal International, v. 109, p. 96 – 105.

Southall, K.E., Gehrels, W.R. and Hayward, B.W., 2006. Foraminifera in a New Zealand salt-marshand their suitability as sea-level indicators. Marine Micropaleontology, v. 60, p. 167 – 179.

Traverse, A., 2007. Paleopalynology. Second Edition, Springer, Dordrecht, p. 1 – 813.

Todd, R. and Bronnimann, P., 1957. Recent Foraminifera and Thecamoebina from the eastern Gulf of Paria. Cushman Foundations for Foraminifera Research, Special Publication no. 3, p. 1 – 43.

Tuovinen, N., Weckstrom, K., and Virtasalo, J.J., 2010. Assessment of recent eutrophication and climate influence in the Archipelago Sea based on the subfossil diatom record. Journal of Paleolimnology, v. 44, p. 95 – 108.

van de Plassche, O.V., 1991. Late Holocene sea-level fluctuations on the shore of Connecticut inferred from transgressive and regressive overlap boundaries in salt-marsh deposits. Journal of Coastal Research, v. 11, p. 159 – 179.

van de Plassche, O.V., Wright, A.J., Horton, B.P., Engelhart, S.E., Kemp, A.C., Mallinson, D., and Kopp, R.E., 2014. Estimating tectonic uplift of the Cape Fear Arch (south-eastern United States) using reconstructions of Holocene relative sea level. Journal of Quaternary Science, v. 29, p. 749 – 759.

Vance, D.J., Culver, S.J., Corbett, D.R., and Buzas, M.A., 2006. Foraminifera in the Albemarle estuarine system, North Carolina: distribution and recent environmental change. Journal of Foraminiferal Research, v. 36, p. 15 – 33.

Walton, W.R., 1952. Techniques for the recognition of living foraminifera. Contributions from the Cushman Foundation for Foraminiferal Research, v. 3, p. 56 – 60.

Wang, T., Surge, D., and Mithen, S., 2012. Seasonal temperature variability of the Neoglacial (3300-2500 BP) and Roman Warm Period (2500-1600 BP) reconstructed from oxygen isotope ratios of limpet shells (*Patella vulgata*), northwest Scotland. Palaeogeography, Palaeoclimatology, Palaeoecology, v. 317-318, p. 104 – 113.

Wang, T., Surge, D., and Walker, K.J., 2013. Seasonal climate change across the Roman Warm Period/Vandal Minimum transition using isotope sclerochronology in archaeological shells and otoliths, southwest Florida, USA. Quaternary International, v. 308-309, p. 230 – 241.

Watcham, E.P., Shennan, I., and Barlow, N.L.M., 2013. Scale considerations in using diatoms as indicators of sea-level change: lessons from Alaska. Journal of Quaternary Science, v. 28, p. 165 – 179.

Wells, J.T. and Kim, S-Y., 1989. Sedimentation in the Albemarle-Pamlico lagoonal system: synthesis and hypotheses. Marine Geology, v. 88, p. 263 – 284.

Woerner, L.S. and Hackney, C.T., 1997. Distribution of *Juncus roemerianus* in North Carolina tidal marshes: the importance of physical and biotic variables. Wetlands, v. 17, p. 284 – 291.

Woodson, A.L., 2012. Reconstructing Holocene Sea Level from Saltmarsh Microfossils, Cedar Island, North Carolina. BA thesis, Bryn Mawr College, p. 1 – 38.

Woodworth, P.L., White, N.J., Jevrejeva, S., Holgate, S.J., Church, J.A., and Gehrels, W.R., 2009. Evidence for the accelerations of sea level on the multi-decade and century timescales. International Journal of Climatology, v. 29, p. 777 – 789.

Zaremba, N., 2014. Holocene stratigraphy and paleoenvironmental change of Pamlico Sound, North Carolina, USA. MS thesis, East Carolina University, p. 1 – 109.

APPENDIX A

Transect 1									
Sampling Station	**Distance (m)**	**Cumulative Distance**	**Vegetation**	**m NAVD88**	**m MLLW**	**m MLW**	**m MTL**	**m MHW**	**m MHHW**
1	0	0	Sand ridge, Juniper pines, shrubs, Iva, some typha	0.265	0.319	0.3075	0.2929	0.2095	0.1867
2	3	3	Typha, some *Spartina cynusoroides* (5%)	0.143	0.197	0.1855	0.1709	0.0875	0.0647
3	3	6	Typha, some *Spartina cynusoroides* (20%)	0.133	0.187	0.1755	0.1609	0.0775	0.0547
4	3	9	70% juncus, 20% *Spartina patens*, 10% *Spartina cynusoroides*	0.134	0.188	0.1765	0.1619	0.0785	0.0557
5	5	14	70% juncus, 20% *Spartina patens*, 10% *Spartina cynusoroides*	0.095	0.149	0.1375	0.1229	0.0395	0.0167
6	10	24	80% Juncus, 20% *Spartina cynusoroides*, some *Spartina patens*	0.109	0.163	0.1515	0.1369	0.0535	0.0307
7	10	34	Upper boundary of monospecific Juncus marsh	0.1	0.154	0.1425	0.1279	0.0445	0.0217
8	15	49	Monospecific Juncus	-0.031	0.023	0.0115	-0.0031	-0.0865	-0.1093
9	15	64	Monospecific Juncus	-0.074	-0.02	-0.0315	-0.0461	-0.1295	-0.1523
10	15	79	Monospecific Juncus	-0.008	0.046	0.0345	0.0199	-0.0635	-0.0863
11	15	94	Monospecific Juncus	0.025	0.079	0.0675	0.0529	-0.0305	-0.0533
12	5	99	Monospecific Juncus	0.027	0.081	0.0695	0.0549	-0.0285	-0.0513
13	1	100	Patch of Distichlis spicata in Juncus stand	0.023	0.077	0.0655	0.0509	-0.0325	-0.0553

Transect 2									
Sampling Station	**Distance (m)**	**Cumulative Distance**	**Vegetation**	**m NAVD88**	**m MLLW**	**m MLW**	**m MTL**	**m MHW**	**m MHHW**
1	0	0	Iva, Juniper pine, shrubs, typha	0.192	0.246	0.2345	0.2199	0.1365	0.1137
2	3	3	Dead typha	0.14	0.194	0.1825	0.1679	0.0845	0.0617
3	5	8	Dead typha	0.136	0.19	0.1785	0.1639	0.0805	0.0577
4	1	9	Dead typha at upper boundary of monospecific Juncus	0.133	0.187	0.1755	0.1609	0.0775	0.0547
5	2	11	Monospecific Juncus	0.066	0.12	0.1085	0.0939	0.0105	-0.0123
6	15	26	Monospecific Juncus	-0.058	-0.004	-0.0155	-0.0301	-0.1135	-0.1363
7	15	41	Monospecific Juncus	-0.063	-0.009	-0.0205	-0.0351	-0.1185	-0.1413
8	15	56	Monospecific Juncus	-0.035	0.019	0.0075	-0.0071	-0.0905	-0.1133
9	15	71	Monospecific Juncus	-0.036	0.018	0.0065	-0.0081	-0.0915	-0.1143

APPENDIX B

Foraminiferal census data: key to taxon names

AI	*Ammoastuta inepta*
AB	*Ammobaculites* spp.
AP	*Ammonia* spp.
As	*Ammotium salsum*
AM	*Arenoparrella mexicana*
EA	*Eggerella advena*
EP	*Elphidium* spp.
HB	*Haplophragmoides bonplandi*
HM	*Haplophragmoides manilaensis*
HW	*Haplophragmoides wilberti*
HG	*Haynesina germanica*
JM	*Jadammina macrescens*
MF	*Miliammina fusca*
MO	*Miliammina obliqua*
MP	*Miliammina petila*
NR	*Nonion radius*
PI	*Polysaccammina ipohalina*
PL	*Pseudothurammina limnetis*
QA	*Quinqueloculina auberiana*
RN	*Reophax nana*
RS	*Reophax scorpiurus*
SL	*Siphotrochammina lobata*
TC	*Tiphotrocha comprimata*
TA	*Trochammina advena*
TI	*Trochammina inflata*
TR	*Trochamminita salsa*

APPENDIX C

Modern foraminiferal census data

Specimen counts

Sample name	AI	AB	AP	As	AM	EA	EP	HB	HM	HW	HG	JM	MF	MO	MP	NR	PI	PL	QA	RN	RS	SL	TC	TA	TI	TR
SHP/TR1/1	0	0	0	0	0	0	0	0	0	0	0	6	4	0	0	0	0	0	0	0	0	0	0	0	0	12
SHP/TR1/2	0	0	0	0	0	0	0	0	0	0	0	0	8	3	0	0	0	2	0	0	0	0	6	0	0	18
SHP/TR1/3	1	0	0	0	1	0	0	0	0	2	0	19	0	1	6	0	0	0	0	0	0	0	33	0	0	42
SHP/TR1/4	0	0	0	0	0	0	0	0	0	1	0	25	4	0	1	0	0	0	0	0	0	0	31	0	0	37
SHP/TR1/5	0	0	0	0	0	0	0	0	0	4	0	39	2	0	3	0	0	0	0	0	0	0	31	0	0	21
SHP/TR1/6	17	0	0	0	1	0	0	0	0	0	0	36	13	0	0	0	0	0	0	0	0	0	7	0	1	15
SHP/TR1/7	0	0	0	0	8	0	0	0	0	0	0	18	0	4	0	0	0	0	0	0	0	0	36	0	18	9
SHP/TR1/8	52	0	0	0	1	0	0	14	1	0	0	12	1	0	0	0	0	0	0	0	0	0	8	0	5	0
SHP/TR1/9	17	0	0	0	0	0	0	0	0	7	0	32	0	0	0	0	0	0	0	0	0	0	46	0	1	0
SHP/TR1/10	16	0	0	0	0	0	2	0	0	0	0	12	0	0	0	0	0	0	0	0	0	2	51	0	18	0
SHP/TR1/11	20	0	1	0	20	0	0	0	0	0	0	3	1	2	1	0	0	0	0	0	0	2	46	0	9	1
SHP/TR1/12	39	0	0	0	18	0	0	0	0	20	0	9	0	0	2	0	0	0	0	0	0	0	3	0	8	2
SHP/TR1/13	44	0	0	0	7	0	0	0	0	8	0	12	3	0	4	0	0	0	0	0	0	2	11	0	4	0
SHP/TR2/1	0	0	0	0	0	0	0	0	0	0	0	18	0	0	0	0	0	0	0	0	0	0	1	0	0	79
SHP/TR2/2	2	0	0	0	0	0	0	0	0	0	0	29	0	3	2	0	0	0	0	0	0	0	13	0	0	46
SHP/TR2/3	5	0	0	0	0	0	0	0	0	0	0	18	1	1	3	0	0	0	0	0	0	0	20	0	0	49
SHP/TR2/4	9	0	0	0	0	0	0	0	0	0	0	17	0	0	1	0	0	1	0	0	0	0	8	0	0	59
SHP/TR2/5	48	0	0	0	0	0	0	0	3	1	0	38	0	0	0	0	0	0	0	0	0	0	8	0	0	1
SHP/TR2/6	12	0	0	0	0	0	0	0	0	0	0	1	0	0	0	0	0	0	0	0	0	0	82	0	3	0
SHP/TR2/7	14	0	0	0	0	0	0	0	0	0	0	7	0	1	0	0	0	0	0	0	0	0	64	0	20	0
SHP/TR2/8	13	0	0	0	0	0	0	1	0	0	0	9	0	0	0	0	0	0	0	0	0	1	61	0	13	0
SHP/TR2/9	26	1	0	0	1	0	0	1	1	2	0	7	1	0	0	0	0	0	0	0	0	2	39	0	11	1
SHP/TR2/10	23	0	0	1	15	0	0	5	0	0	0	6	0	1	0	0	0	0	0	0	0	2	34	0	6	0

Relative percent abundance

Sample name	AI	AB	AP	As	AM	EA	EP	HB	HM	HW	HG	JM	MF
SHP/TR1/1	0.0	0.0	0.0	0.0	0.0	0.0	0.0	0.0	0.0	0.0	0.0	27.3	18.2
SHP/TR1/2	0.0	0.0	0.0	0.0	0.0	0.0	0.0	0.0	0.0	0.0	0.0	0.0	21.7
SHP/TR1/3	1.0	0.0	0.0	0.0	1.0	0.0	0.0	0.0	0.0	2.0	0.0	18.0	0.0
SHP/TR1/4	0.0	0.0	0.0	0.0	0.0	0.0	0.0	0.0	0.0	1.3	0.0	25.0	3.8
SHP/TR1/5	0.0	0.0	0.0	0.0	0.0	0.0	0.0	0.0	0.0	4.2	0.0	38.5	2.1
SHP/TR1/6	19.2	0.0	0.0	0.0	1.3	0.0	0.0	0.0	0.0	0.0	0.0	39.7	14.1
SHP/TR1/7	0.0	0.0	0.0	0.0	8.6	0.0	0.0	0.0	0.0	0.0	0.0	19.4	0.0
SHP/TR1/8	54.3	0.0	0.0	0.0	1.4	0.0	0.0	14.3	1.4	0.0	0.0	12.9	1.4
SHP/TR1/9	16.7	0.0	0.0	0.0	0.0	0.0	0.0	0.0	0.0	6.4	0.0	30.8	0.0
SHP/TR1/10	15.7	0.0	0.0	0.0	0.0	0.0	2.0	0.0	0.0	0.0	0.0	11.8	0.0
SHP/TR1/11	18.4	0.0	1.0	0.0	18.4	0.0	0.0	0.0	0.0	0.0	0.0	2.9	1.0
SHP/TR1/12	38.7	0.0	0.0	0.0	18.3	0.0	0.0	0.0	0.0	19.4	0.0	8.6	0.0
SHP/TR1/13	46.5	0.0	0.0	0.0	7.1	0.0	0.0	0.0	0.0	8.1	0.0	13.1	3.0
SHP/TR2/1	0.0	0.0	0.0	0.0	0.0	0.0	0.0	0.0	0.0	0.0	0.0	18.5	0.0
SHP/TR2/2	2.2	0.0	0.0	0.0	0.0	0.0	0.0	0.0	0.0	0.0	0.0	30.0	0.0
SHP/TR2/3	5.4	0.0	0.0	0.0	0.0	0.0	0.0	0.0	0.0	0.0	0.0	18.5	1.1
SHP/TR2/4	9.6	0.0	0.0	0.0	0.0	0.0	0.0	0.0	0.0	0.0	0.0	18.1	0.0
SHP/TR2/5	48.3	0.0	0.0	0.0	0.0	0.0	0.0	0.0	3.4	1.1	0.0	37.9	0.0
SHP/TR2/6	12.1	0.0	0.0	0.0	0.0	0.0	0.0	0.0	0.0	0.0	0.0	1.5	0.0
SHP/TR2/7	13.3	0.0	0.0	0.0	0.0	0.0	0.0	0.0	0.0	0.0	0.0	6.7	0.0
SHP/TR2/8	13.2	0.0	0.0	0.0	0.0	0.0	0.0	1.5	0.0	0.0	0.0	8.8	0.0
SHP/TR2/9	28.1	1.1	0.0	0.0	1.1	0.0	0.0	1.1	1.1	2.2	0.0	7.9	1.1
SHP/TR2/10	24.2	0.0	0.0	1.1	16.5	0.0	0.0	5.5	0.0	0.0	0.0	6.6	0.0

Sample name	MO	MP	NR	PI	PL	QA	RN	RS	SL	TC	TA	TI	TR	Total
SHP/TR1/1	0.0	0.0	0.0	0.0	0.0	0.0	0.0	0.0	0.0	0.0	0.0	0.0	54.5	100.0
SHP/TR1/2	8.7	0.0	0.0	0.0	4.3	0.0	0.0	0.0	0.0	17.4	0.0	0.0	47.8	100.0
SHP/TR1/3	1.0	6.0	0.0	0.0	0.0	0.0	0.0	0.0	0.0	31.0	0.0	0.0	40.0	100.0
SHP/TR1/4	0.0	1.3	0.0	0.0	0.0	0.0	0.0	0.0	0.0	31.3	0.0	0.0	37.5	100.0
SHP/TR1/5	0.0	3.1	0.0	0.0	0.0	0.0	0.0	0.0	0.0	31.3	0.0	0.0	20.8	100.0
SHP/TR1/6	0.0	0.0	0.0	0.0	0.0	0.0	0.0	0.0	0.0	7.7	0.0	1.3	16.7	100.0
SHP/TR1/7	4.3	0.0	0.0	0.0	0.0	0.0	0.0	0.0	0.0	38.7	0.0	19.4	9.7	100.0
SHP/TR1/8	0.0	0.0	0.0	0.0	0.0	0.0	0.0	0.0	0.0	8.6	0.0	5.7	0.0	100.0
SHP/TR1/9	0.0	0.0	0.0	0.0	0.0	0.0	0.0	0.0	0.0	44.9	0.0	1.3	0.0	100.0
SHP/TR1/10	0.0	0.0	0.0	0.0	0.0	0.0	0.0	0.0	2.0	51.0	0.0	17.6	0.0	100.0
SHP/TR1/11	1.9	1.0	0.0	0.0	0.0	0.0	0.0	0.0	1.9	43.7	0.0	8.7	1.0	100.0
SHP/TR1/12	0.0	2.2	0.0	0.0	0.0	0.0	0.0	0.0	0.0	3.2	0.0	7.5	2.2	100.0
SHP/TR1/13	0.0	4.0	0.0	0.0	0.0	0.0	0.0	0.0	2.0	12.1	0.0	4.0	0.0	100.0
SHP/TR2/1	0.0	0.0	0.0	0.0	0.0	0.0	0.0	0.0	0.0	1.1	0.0	0.0	80.4	100.0
SHP/TR2/2	3.3	2.2	0.0	0.0	0.0	0.0	0.0	0.0	0.0	13.3	0.0	0.0	48.9	100.0
SHP/TR2/3	1.1	3.3	0.0	0.0	0.0	0.0	0.0	0.0	0.0	20.7	0.0	0.0	50.0	100.0
SHP/TR2/4	0.0	1.1	0.0	0.0	1.1	0.0	0.0	0.0	0.0	8.5	0.0	0.0	61.7	100.0
SHP/TR2/5	0.0	0.0	0.0	0.0	0.0	0.0	0.0	0.0	0.0	8.0	0.0	0.0	1.1	100.0
SHP/TR2/6	0.0	0.0	0.0	0.0	0.0	0.0	0.0	0.0	0.0	83.3	0.0	3.0	0.0	100.0
SHP/TR2/7	1.3	0.0	0.0	0.0	0.0	0.0	0.0	0.0	0.0	60.0	0.0	18.7	0.0	100.0
SHP/TR2/8	0.0	0.0	0.0	0.0	0.0	0.0	0.0	0.0	1.5	61.8	0.0	13.2	0.0	100.0
SHP/TR2/9	0.0	0.0	0.0	0.0	0.0	0.0	0.0	0.0	2.2	41.6	0.0	11.2	1.1	100.0
SHP/TR2/10	1.1	0.0	0.0	0.0	0.0	0.0	0.0	0.0	2.2	36.3	0.0	6.6	0.0	100.0

APPENDIX D

Original references to Sand Hill Point taxa identified to the species level

Ammoastuta inepta (Cushman and McCulloch) = *Ammoastuta ineptus* Cushman and McCulloch, 1939, p. 89, pl. 7, fig. 6.

Ammobaculites exigus. Cushman and Bronnimann, 1948b, p. 38, pl. 7, figs. 7, 8.

Ammotium salsum Cushman and Bronnimann, 1948a, p. 16, pl. 3, figs. 7 – 9.

Arenoparrella mexicana (Kornfeld) = *Trochammina inflata* (Montagu) var. *mexicana* Kornfeld, 1931, p. 86, pl. 13, fig. 5.

Haplophragmoides bonplandi Todd and Bronnimann, 1957, p. 23, pl. 3, fig. 2.

Haplophragmoides manilaensis. Andersen, 1953, p. 22, pl. 4, fig. 7.

Haplophragmoides wilberti Andersen, 1953, p. 21, pl. 4, fig. 7.

Jadammina macrescens (Brady) = *Trochammina inflata* (Montagu) var. *macrescens* Brady, in Brady and Robertson, 1870, p. 47, pl. 11, figs. 5a – c.

Miliammina fusca (Brady) = *Quinqueloculina fusca* Brady, in Brady and Robertson, 1870, p. 47, pl. 11, figs. 2, 3.

Miliammina obliqua Heron-Allen and Earland, 1930, p. 42, pl. 1, figs. 7 – 12.

Miliammina petila Saunders, 1958, p. 88, pl. 1, fig. 15.

Pseudoammina limnetis (Scott and Medioli) = *Thurammina (?) limnetis* Scott and Medioli, 1980, p. 43, pl. 1, figs. 1 – 3.

Siphotrochammina lobata Saunders, 1957, p. 9, 10, pl. 3, figs. 1, 2.

Tiphotrocha comprimata (Cushman and Bronnimann) = *Trochammina comprimata* Cushman and Bronnimann, 1948b, p. 41, pl. 8, figs. 1 – 3.

Trochammina inflata (Montagu) = *Nautilus inflatus.* Montagu, 1808, p. 81, pl. 18, fig. 3.

Trochamminita salsa (Cushman and Bronnimann) = *Labrospira salsa* Cushman and Bronnimann, 1948a, p. 16, pl. 3, figs. 5, 6.

APPENDIX E

Radiocarbon data

As received from National Ocean Sciences AMS (NOSAMS) Facility

Date Reported	Submitter Identification	Type	Process	Accession #	F Modern	Fm Err	Age	Age Err	$\delta^{13}C$	$\delta^{13}C$ Source	$\delta^{14}C$
12/23/2013	SHP-9/88cm	Plant/Wood	Organic Carbon	OS-107656	0.9253	0.0034	625	30	-27.19	MEASURED	-81.6
12/23/2013	SHP-9/98cm	Plant/Wood	Organic Carbon	OS-107657	0.9188	0.0028	680	25	-26.66	MEASURED	-88.04
12/23/2013	SHP-9/110cm	Plant/Wood	Organic Carbon	OS-107658	0.8859	0.0034	975	30	-27.39	MEASURED	-120.74
6/3/2014	SHP-9 124cm*	Plant/Wood	Organic Carbon	OS-110628	0.8633	0.0027	1,180	25	-24.53	MEASURED	-143.19
12/23/2013	SHP-9/139cm	Plant/Wood	Organic Carbon	OS-107659	0.8354	0.0024	1,440	25	-27.55	MEASURED	-170.83
12/23/2013	SHP-9/153cm	Plant/Wood	Organic Carbon	OS-107661	0.8292	0.0023	1,500	20	-28.22	MEASURED	-177.02
12/23/2013	SHP-9/166cm	Plant/Wood	Organic Carbon	OS-107662	0.9744	0.0034	210	25	-25.97	MEASURED	-32.89
12/23/2013	SHP-9/177cm	Plant/Wood	Organic Carbon	OS-107663	0.7912	0.0024	1,880	25	-14.5	MEASURED	-214.71
1/6/2014	SHP-9/206cm	Plant/Wood	Organic Carbon	OS-107768	0.7620	0.0025	2,180	25	-28.77	MEASURED	-243.71
6/3/2014	SHP-9 226cm*	Plant/Wood	Organic Carbon	OS-110629	0.7695	0.0023	2,100	25	-27.57	MEASURED	-236.23
1/7/2014	SHP-9/246cm	Charcoal	Organic Carbon	OS-107785	0.6484	0.0021	3,480	25	-26.3	MEASURED	-356.44
1/7/2014	SHP-9/267cm	Plant/Wood	Organic Carbon	OS-107786	0.5363	0.0024	5,000	35	-26.54	MEASURED	-467.73

* The asterisks indicate that the radiocarbon result was corrected for isotopic fractionation using unreported $d^{13}C$ values measured on the accelerator.

APPENDIX F

Down-core foraminiferal census data

Specimen counts

Sample Depth	AI	AB	AP	As	AM	EA	EP	HB	HW	HM	HG	JM	MF
82	34	0	0	0	44	0	1	0	1	0	0	6	0
86	5	1	0	0	72	0	0	2	1	0	0	0	0
90	2	0	0	0	33	0	0	0	0	0	0	12	0
94	8	0	0	1	6	0	2	0	0	3	0	17	0
98	26	1	0	0	28	0	0	0	0	0	0	3	1
102	26	0	0	0	33	0	0	0	0	0	0	13	0
106	18	0	0	0	43	0	2	3	0	0	0	7	0
110	21	0	0	0	11	0	0	0	0	0	0	10	0
114	12	0	0	0	0	0	0	0	0	0	0	18	0
118	37	2	0	0	4	0	0	0	1	0	0	12	0
121	40	0	0	0	14	0	0	0	0	1	0	19	0
123	26	0	0	0	13	0	0	0	1	1	0	7	0
125	17	0	0	0	14	0	0	0	2	1	0	13	0
127	7	0	0	0	14	0	0	1	4	0	0	14	0
129	15	0	0	0	11	0	1	0	1	0	0	14	0
132	14	0	0	0	9	0	0	0	0	1	0	22	0
136	15	0	0	0	3	0	0	0	1	0	0	15	2
140	18	1	0	0	7	0	0	0	0	0	0	17	0
144	20	0	0	0	9	0	0	0	0	0	0	23	0
148	13	0	0	0	11	0	1	0	0	0	0	11	0
152	17	0	0	0	13	0	0	0	0	0	0	22	1
156	23	0	0	0	13	0	0	0	1	0	0	20	0
160	41	0	0	0	9	0	0	0	0	0	0	43	0
163	38	0	0	0	6	0	1	0	0	0	0	48	0
165	47	0	0	0	9	0	0	0	1	0	0	28	1
167	29	0	0	0	15	0	0	0	1	0	0	33	0
169	17	0	1	0	30	0	1	0	1	0	0	16	1
172	37	0	0	0	14	0	1	0	0	0	0	35	1
176	49	0	0	0	10	0	0	0	1	0	0	23	0
180	26	0	0	0	28	0	0	0	5	4	0	8	1
184	26	0	0	0	18	0	7	1	0	6	0	14	1
188	27	0	0	0	32	0	0	1	0	0	0	7	0
192	17	0	0	0	57	0	0	0	1	0	0	7	1
196	23	1	0	0	46	0	0	3	1	0	0	10	0
200	19	0	0	0	32	0	0	1	0	0	0	17	4
202	12	0	0	0	23	0	0	1	2	0	0	10	0
204	22	0	0	0	29	0	0	0	0	6	0	6	1
206	19	0	0	0	22	0	0	2	2	2	0	4	0
208	15	0	0	0	42	0	0	0	3	2	0	8	3
210	36	0	0	1	20	0	0	1	7	1	0	4	0
214	21	0	0	0	11	0	0	2	0	2	0	7	0
218	5	0	0	0	11	0	0	0	1	0	0	0	0
222	25	0	0	0	22	0	2	1	2	3	0	10	0
226	5	0	0	0	4	0	0	0	2	0	0	1	0
230	5	0	0	0	12	0	0	0	0	0	0	0	0

Sample Depth	MO	MP	NR	PI	PL	QA	RN	RS	SL	TC	TA	TI	TR
82	0	0	0	0	0	0	0	0	2	14	0	0	0
86	0	0	0	0	0	0	0	0	0	17	0	2	0
90	0	0	0	0	0	0	0	0	8	32	0	10	0
94	0	0	0	0	0	0	0	0	19	38	0	3	0
98	0	0	0	0	0	0	0	0	9	23	0	6	0
102	0	0	0	0	0	0	0	0	2	20	0	1	0
106	0	1	0	0	0	0	0	0	6	18	0	2	0
110	0	0	0	0	0	0	0	0	7	44	0	4	0
114	0	1	0	0	0	0	0	0	12	51	0	1	0
118	0	0	0	0	0	0	0	0	6	32	0	3	0
121	0	0	0	0	0	0	0	0	0	17	0	4	0
123	0	0	0	0	0	0	0	0	6	36	0	6	0
125	0	0	0	0	0	0	0	0	10	29	0	5	0
127	0	0	0	0	0	0	0	0	7	20	0	5	0
129	0	0	0	0	0	0	0	0	3	13	0	3	0
132	0	0	0	0	0	0	0	0	19	31	0	6	0
136	0	0	0	0	0	0	0	0	3	49	0	2	0
140	0	1	0	0	0	0	0	0	6	40	0	4	0
144	0	0	0	0	0	0	0	0	8	36	0	0	0
148	0	0	0	0	0	0	0	0	23	31	0	7	0
152	0	0	0	0	0	0	0	0	16	16	0	4	0
156	0	0	0	0	0	0	0	0	12	22	0	2	0
160	0	0	0	0	0	0	0	0	2	3	0	2	0
163	0	0	0	0	0	0	0	0	2	4	0	2	0
165	0	0	0	0	0	0	0	0	2	2	0	1	0
167	0	1	0	0	0	0	0	0	9	4	0	4	0
169	0	0	0	0	0	0	0	0	8	24	0	4	0
172	0	0	0	0	0	0	0	0	6	6	0	2	0
176	0	0	0	0	0	0	0	0	3	9	0	1	0
180	0	3	0	0	0	0	0	0	5	17	0	4	0
184	0	2	0	0	0	0	0	0	9	11	0	3	0
188	0	0	0	0	0	0	0	0	5	22	0	0	0
192	0	0	0	0	0	0	0	0	10	8	0	1	0
196	0	0	0	0	0	0	0	0	5	11	0	1	0
200	0	0	0	0	0	0	0	0	11	15	0	0	0
202	0	2	0	0	1	0	0	0	11	7	0	0	0
204	0	1	0	0	0	0	0	0	6	25	0	3	0
206	0	4	0	0	0	0	0	0	6	29	0	7	0
208	0	0	0	0	0	0	0	0	4	19	0	4	0
210	0	0	0	0	0	0	0	0	2	24	0	3	0
214	0	0	0	0	0	0	0	0	6	10	0	1	0
218	0	0	0	0	0	0	0	0	1	7	0	0	0
222	0	3	0	0	0	0	0	0	15	7	0	4	0
226	0	0	0	0	0	0	0	0	1	2	0	0	0
230	0	0	0	0	0	0	0	0	3	7	0	3	0

Relative percent abundance

Sample Depth	AI	AB	AP	As	AM	EA	EP	HB	HM	HW	HG	JM	MF
82	33.3	0.0	0.0	0.0	43.1	0.0	1.0	0.0	0.0	1.0	0.0	5.9	0.0
86	5.0	1.0	0.0	0.0	72.0	0.0	0.0	2.0	0.0	1.0	0.0	0.0	0.0
90	2.1	0.0	0.0	0.0	34.0	0.0	0.0	0.0	0.0	0.0	0.0	12.4	0.0
94	8.2	0.0	0.0	1.0	6.2	0.0	2.1	0.0	3.1	0.0	0.0	17.5	0.0
98	26.8	1.0	0.0	0.0	28.9	0.0	0.0	0.0	0.0	0.0	0.0	3.1	1.0
102	27.4	0.0	0.0	0.0	34.7	0.0	0.0	0.0	0.0	0.0	0.0	13.7	0.0
106	18.0	0.0	0.0	0.0	43.0	0.0	2.0	3.0	0.0	0.0	0.0	7.0	0.0
110	21.6	0.0	0.0	0.0	11.3	0.0	0.0	0.0	0.0	0.0	0.0	10.3	0.0
114	12.6	0.0	0.0	0.0	0.0	0.0	0.0	0.0	0.0	0.0	0.0	18.9	0.0
118	38.1	2.1	0.0	0.0	4.1	0.0	0.0	0.0	0.0	1.0	0.0	12.4	0.0
121	41.2	0.0	0.0	0.0	14.4	0.0	0.0	0.0	1.0	0.0	0.0	19.6	0.0
123	27.1	0.0	0.0	0.0	13.5	0.0	0.0	0.0	1.0	1.0	0.0	7.3	0.0
125	18.7	0.0	0.0	0.0	15.4	0.0	0.0	0.0	1.1	2.2	0.0	14.3	0.0
127	9.7	0.0	0.0	0.0	19.4	0.0	0.0	1.4	0.0	5.6	0.0	19.4	0.0
129	24.6	0.0	0.0	0.0	18.0	0.0	1.6	0.0	0.0	1.6	0.0	23.0	0.0
132	13.7	0.0	0.0	0.0	8.8	0.0	0.0	0.0	1.0	0.0	0.0	21.6	0.0
136	16.7	0.0	0.0	0.0	3.3	0.0	0.0	0.0	0.0	1.1	0.0	16.7	2.2
140	19.1	1.1	0.0	0.0	7.4	0.0	0.0	0.0	0.0	0.0	0.0	18.1	0.0
144	20.8	0.0	0.0	0.0	9.4	0.0	0.0	0.0	0.0	0.0	0.0	24.0	0.0
148	13.4	0.0	0.0	0.0	11.3	0.0	1.0	0.0	0.0	0.0	0.0	11.3	0.0
152	19.1	0.0	0.0	0.0	14.6	0.0	0.0	0.0	0.0	0.0	0.0	24.7	1.1
156	24.7	0.0	0.0	0.0	14.0	0.0	0.0	0.0	0.0	1.1	0.0	21.5	0.0
160	41.0	0.0	0.0	0.0	9.0	0.0	0.0	0.0	0.0	0.0	0.0	43.0	0.0
163	37.6	0.0	0.0	0.0	5.9	0.0	1.0	0.0	0.0	0.0	0.0	47.5	0.0
165	51.6	0.0	0.0	0.0	9.9	0.0	0.0	0.0	0.0	1.1	0.0	30.8	1.1
167	30.2	0.0	0.0	0.0	15.6	0.0	0.0	0.0	0.0	1.0	0.0	34.4	0.0
169	16.5	0.0	1.0	0.0	29.1	0.0	1.0	0.0	0.0	1.0	0.0	15.5	1.0
172	36.3	0.0	0.0	0.0	13.7	0.0	1.0	0.0	0.0	0.0	0.0	34.3	1.0
176	51.0	0.0	0.0	0.0	10.4	0.0	0.0	0.0	0.0	1.0	0.0	24.0	0.0
180	25.7	0.0	0.0	0.0	27.7	0.0	0.0	0.0	4.0	5.0	0.0	7.9	1.0
184	26.5	0.0	0.0	0.0	18.4	0.0	7.1	1.0	6.1	0.0	0.0	14.3	1.0
188	28.7	0.0	0.0	0.0	34.0	0.0	0.0	1.1	0.0	0.0	0.0	7.4	0.0
192	16.7	0.0	0.0	0.0	55.9	0.0	0.0	0.0	0.0	1.0	0.0	6.9	1.0
196	22.8	1.0	0.0	0.0	45.5	0.0	0.0	3.0	0.0	1.0	0.0	9.9	0.0
200	19.2	0.0	0.0	0.0	32.3	0.0	0.0	1.0	0.0	0.0	0.0	17.2	4.0
202	17.4	0.0	0.0	0.0	33.3	0.0	0.0	1.4	0.0	2.9	0.0	14.5	0.0
204	22.2	0.0	0.0	0.0	29.3	0.0	0.0	0.0	6.1	0.0	0.0	6.1	1.0
206	19.6	0.0	0.0	0.0	22.7	0.0	0.0	2.1	2.1	2.1	0.0	4.1	0.0
208	15.0	0.0	0.0	0.0	42.0	0.0	0.0	0.0	2.0	3.0	0.0	8.0	3.0
210	36.0	0.0	0.0	1.0	20.0	0.0	0.0	1.0	1.0	7.0	0.0	4.0	0.0
214	35.0	0.0	0.0	0.0	18.3	0.0	0.0	3.3	3.3	0.0	0.0	11.7	0.0
218	20.0	0.0	0.0	0.0	44.0	0.0	0.0	0.0	0.0	4.0	0.0	0.0	0.0
222	26.6	0.0	0.0	0.0	23.4	0.0	2.1	1.1	3.2	2.1	0.0	10.6	0.0
226	33.3	0.0	0.0	0.0	26.7	0.0	0.0	0.0	0.0	13.3	0.0	6.7	0.0
230	16.7	0.0	0.0	0.0	40.0	0.0	0.0	0.0	0.0	0.0	0.0	0.0	0.0

Sample Depth	MO	MP	NR	PI	PL	QA	RN	RS	SL	TC	TA	TI	TR	Total
82	0.0	0.0	0.0	0.0	0.0	0.0	0.0	0.0	2.0	13.7	0.0	0.0	0.0	100.0
86	0.0	0.0	0.0	0.0	0.0	0.0	0.0	0.0	0.0	17.0	0.0	2.0	0.0	100.0
90	0.0	0.0	0.0	0.0	0.0	0.0	0.0	0.0	8.2	33.0	0.0	10.3	0.0	100.0
94	0.0	0.0	0.0	0.0	0.0	0.0	0.0	0.0	19.6	39.2	0.0	3.1	0.0	100.0
98	0.0	0.0	0.0	0.0	0.0	0.0	0.0	0.0	9.3	23.7	0.0	6.2	0.0	100.0
102	0.0	0.0	0.0	0.0	0.0	0.0	0.0	0.0	2.1	21.1	0.0	1.1	0.0	100.0
106	0.0	1.0	0.0	0.0	0.0	0.0	0.0	0.0	6.0	18.0	0.0	2.0	0.0	100.0
110	0.0	0.0	0.0	0.0	0.0	0.0	0.0	0.0	7.2	45.4	0.0	4.1	0.0	100.0
114	0.0	1.1	0.0	0.0	0.0	0.0	0.0	0.0	12.6	53.7	0.0	1.1	0.0	100.0
118	0.0	0.0	0.0	0.0	0.0	0.0	0.0	0.0	6.2	33.0	0.0	3.1	0.0	100.0
121	0.0	0.0	0.0	0.0	0.0	0.0	0.0	0.0	0.0	17.5	0.0	4.1	0.0	100.0
123	0.0	0.0	0.0	0.0	0.0	0.0	0.0	0.0	6.3	37.5	0.0	6.3	0.0	100.0
125	0.0	0.0	0.0	0.0	0.0	0.0	0.0	0.0	11.0	31.9	0.0	5.5	0.0	100.0
127	0.0	0.0	0.0	0.0	0.0	0.0	0.0	0.0	9.7	27.8	0.0	6.9	0.0	100.0
129	0.0	0.0	0.0	0.0	0.0	0.0	0.0	0.0	4.9	21.3	0.0	4.9	0.0	100.0
132	0.0	0.0	0.0	0.0	0.0	0.0	0.0	0.0	18.6	30.4	0.0	5.9	0.0	100.0
136	0.0	0.0	0.0	0.0	0.0	0.0	0.0	0.0	3.3	54.4	0.0	2.2	0.0	100.0
140	0.0	1.1	0.0	0.0	0.0	0.0	0.0	0.0	6.4	42.6	0.0	4.3	0.0	100.0
144	0.0	0.0	0.0	0.0	0.0	0.0	0.0	0.0	8.3	37.5	0.0	0.0	0.0	100.0
148	0.0	0.0	0.0	0.0	0.0	0.0	0.0	0.0	23.7	32.0	0.0	7.2	0.0	100.0
152	0.0	0.0	0.0	0.0	0.0	0.0	0.0	0.0	18.0	18.0	0.0	4.5	0.0	100.0
156	0.0	0.0	0.0	0.0	0.0	0.0	0.0	0.0	12.9	23.7	0.0	2.2	0.0	100.0
160	0.0	0.0	0.0	0.0	0.0	0.0	0.0	0.0	2.0	3.0	0.0	2.0	0.0	100.0
163	0.0	0.0	0.0	0.0	0.0	0.0	0.0	0.0	2.0	4.0	0.0	2.0	0.0	100.0
165	0.0	0.0	0.0	0.0	0.0	0.0	0.0	0.0	2.2	2.2	0.0	1.1	0.0	100.0
167	0.0	1.0	0.0	0.0	0.0	0.0	0.0	0.0	9.4	4.2	0.0	4.2	0.0	100.0
169	0.0	0.0	0.0	0.0	0.0	0.0	0.0	0.0	7.8	23.3	0.0	3.9	0.0	100.0
172	0.0	0.0	0.0	0.0	0.0	0.0	0.0	0.0	5.9	5.9	0.0	2.0	0.0	100.0
176	0.0	0.0	0.0	0.0	0.0	0.0	0.0	0.0	3.1	9.4	0.0	1.0	0.0	100.0
180	0.0	3.0	0.0	0.0	0.0	0.0	0.0	0.0	5.0	16.8	0.0	4.0	0.0	100.0
184	0.0	2.0	0.0	0.0	0.0	0.0	0.0	0.0	9.2	11.2	0.0	3.1	0.0	100.0
188	0.0	0.0	0.0	0.0	0.0	0.0	0.0	0.0	5.3	23.4	0.0	0.0	0.0	100.0
192	0.0	0.0	0.0	0.0	0.0	0.0	0.0	0.0	9.8	7.8	0.0	1.0	0.0	100.0
196	0.0	0.0	0.0	0.0	0.0	0.0	0.0	0.0	5.0	10.9	0.0	1.0	0.0	100.0
200	0.0	0.0	0.0	0.0	0.0	0.0	0.0	0.0	11.1	15.2	0.0	0.0	0.0	100.0
202	0.0	2.9	0.0	0.0	1.4	0.0	0.0	0.0	15.9	10.1	0.0	0.0	0.0	100.0
204	0.0	1.0	0.0	0.0	0.0	0.0	0.0	0.0	6.1	25.3	0.0	3.0	0.0	100.0
206	0.0	4.1	0.0	0.0	0.0	0.0	0.0	0.0	6.2	29.9	0.0	7.2	0.0	100.0
208	0.0	0.0	0.0	0.0	0.0	0.0	0.0	0.0	4.0	19.0	0.0	4.0	0.0	100.0
210	0.0	0.0	0.0	0.0	0.0	0.0	0.0	0.0	2.0	24.0	0.0	3.0	0.0	100.0
214	0.0	0.0	0.0	0.0	0.0	0.0	0.0	0.0	10.0	16.7	0.0	1.7	0.0	100.0
218	0.0	0.0	0.0	0.0	0.0	0.0	0.0	0.0	4.0	28.0	0.0	0.0	0.0	100.0
222	0.0	3.2	0.0	0.0	0.0	0.0	0.0	0.0	16.0	7.4	0.0	4.3	0.0	100.0
226	0.0	0.0	0.0	0.0	0.0	0.0	0.0	0.0	6.7	13.3	0.0	0.0	0.0	100.0
230	0.0	0.0	0.0	0.0	0.0	0.0	0.0	0.0	10.0	23.3	0.0	10.0	0.0	100.0

APPENDIX G

Pollen data

Christopher Bernhardt, Research Geologist, U.S. Geological Survey, Personal Communication, December, 2014

Palynomorphs (pollen and fern spores) were isolated from ten samples using standard palynological preparation techniques (Traverse, 2007) at the U.S. Geological Survey (Reston, Virginia). For each sample, one tablet of *Lycopodium* spores was added to approximately 3 g dry sediment to calculate palynomorph concentration (grains g^{-1}). At least 300 pollen grains and spores were counted from each sample to determine percent abundance and concentration of palynomorphs. Identification was aided by slides from the United States Geological Survey (Reston, Virginia). Pollen abundance is based on the sum of both pollen and fern spores.

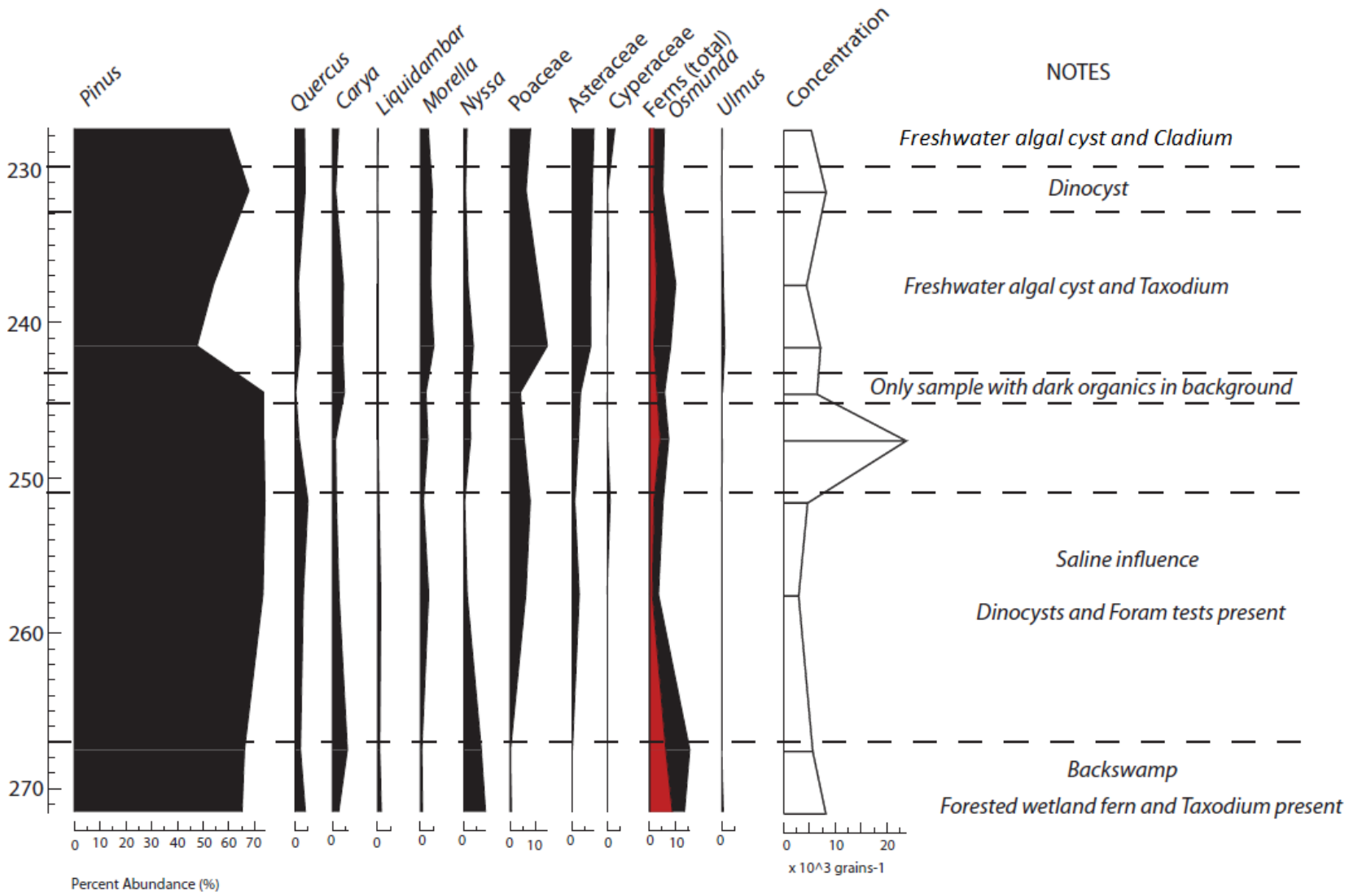

Figure 1: Pollen abundance for Core SHP-9A for 225 – 275 cm depth. Reproduced from Bernhardt, C., personal communication, December 2014.

APPENDIX H

Impact of the presence/absence of *Tiphotrocha comprimata* on standardized water level index values using a locally weighted weighted average (LWWA) transfer function (Bray-Curtis percent dissimilarity distance metric, *k* values of 50)

Sample Depth	SWLI value for all species	SWLI value for all species excluding *Tiphotrocha comprimata*
82	87.49	89.90
86	102.56	97.96
90	88.35	118.76
94	64.93	93.77
98	72.91	80.70
102	85.40	99.20
106	79.80	92.09
110	53.12	102.09
114	45.89	68.82
118	59.47	68.99
121	83.84	80.68
123	62.35	103.10
125	77.10	100.14
127	88.23	124.28
129	92.59	104.48
132	71.61	102.01
136	46.34	83.66
140	57.00	75.71
144	62.30	93.61
148	70.97	107.74
152	84.95	100.87
156	75.71	96.38
160	115.36	90.63
163	118.62	89.38
165	103.79	86.29
167	116.20	91.30
169	83.49	113.34
172	109.09	88.69
176	92.29	85.66
180	100.50	125.12
184	97.21	109.85
188	75.22	98.27
192	99.71	105.08
196	88.51	100.17
200	93.08	107.96
202	99.80	106.62
204	79.87	102.76
206	74.21	111.02
208	92.60	109.06
210	76.60	95.62
214	84.27	101.02
218	76.02	100.49
222	100.19	117.77
226	97.54	118.31
230	76.69	96.34

APPENDIX I

Concepts involved in sea-level reconstructions

I. Salt-marsh zonation and sea-level indicators

Salt-marshes in coastal regions such as North Carolina tend to exhibit a distinct plant zonation (Gehrels, 1994) separated into low- and high-marsh zones. Not unlike salt-marsh plants, salt-marsh foraminifera exhibit distinct zonation in many marshes (e.g., Gehrels, 1994; Guilbault, 1996; Horton and Edwards, 2006). This zonation, along with the tendency of salt-marsh foraminifera to be abundant and exhibit low diversity, allows for foraminifera to be used as a proxy for elevation and, hence, tidal inundation.

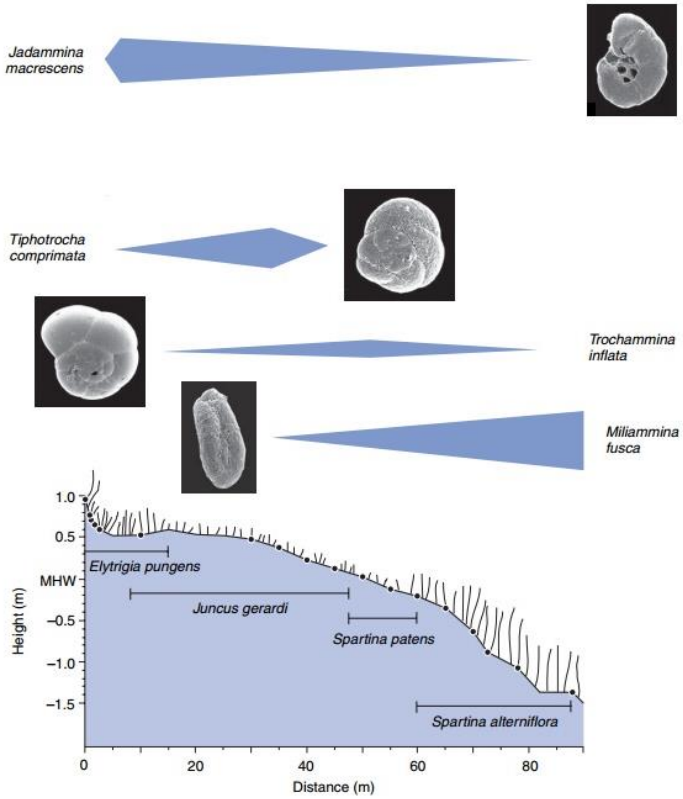

Figure 2: Distribution of typical salt-marsh foraminifera and salt-marsh plants with distance. At Cedar Island, salt-marsh plant distribution tends to shift from a small border of *Spartina alterniflora* at the marsh edge to an overwhelmingly dominant zone of *Juncus roemerianus* (with patches of *Distichlis spicata*) due to its limited elevation range (~0.11 m). Reproduced from Gehrels (2007).

a. Sea-level indicators and index points

The indicative meaning of a sample is the difference between the reference water level (RWL) and the indicative range for a particular sample. In terms of sea-level reconstructions, a sea-level indicator is anything that can be used as a proxy of former sea-level variations. Index points relate sea level at one time at one elevation. In order to have a valid index point for sea-level reconstructions from a salt-marsh, it must systematically be related to tides. For a sea-level index point to be established, a former sea-level indicator is dated, its height is measured, and the height relative to sea level of its modern counterpart (indicative meaning) is known (Gehrels, 2007). The indicative meaning refers to the height of a sea-level indicator in the modern environment as measured related to a tide level. Salt-marsh foraminifera are especially useful in this aspect for sea-level reconstructions because they preserved well in the fossil sediments and many have a world-wide distribution (Gehrels, 2007).

II. Transfer function

a. Modern training set

Development of the modern training set involves the pairing of observations of foraminiferal assemblages, which determine the relative abundances of species from the modern environment. It is assumed that the modern environment of these assemblages are analogous to preserved assemblages. Data from multiple studies can be merged to conveniently generate larger training sets (Kemp and Telford, 2015). The twenty-three surface samples and associated elevational data from Sand Hill Point were added to the regional dataset which was employed as the training set. The strongest relationship between foraminiferal assemblage and elevation is expressed in the highest samples at the uppermost limit of marine influence. At Sand Hill Point these samples tend to be nearly monospecific, dominated by *Trochamminita salsa.*

b. Dissimilarity

While evaluating the modern analogs, the greater the dissimilarity between a down-core assemblage and samples in the training set, the more the transfer function is forced to extrapolate, which increases the resultant error (Horton and Edwards, 2006). Dissimilarity can be calculated using a selected metric including Bray-Curtis percent dissimilarity, Squared chord distance, Squared chi-square distance, and Squared Euclidean distance

c. Numerical methods

Development of the transfer function requires the selection of an appropriate numerical technique to define the relationship between foraminiferal species and tidal elevation. The most common numerical methods used for sea-level research (Kemp and Telford, 2015) using different approaches include: Maximum Likelihood, Weighted Averaging, Weighted Averaging Partial Least Squares (WA-PLS), Modern Analogue Technique (MAT), and Locally Weighted Weighted Averaging (LWWA).

Maximum Likelihood is a classical approach where one environmental variable is regressed with one species. However, it is strongly influenced by outliers and zero values in both the modern and fossil dataset (Kemp and Telford, 2015), which occurs frequently in the North Carolina regional dataset. The WA method treats the environmental variable as the response and the species as the predictor, acting as in inverse model. This method often relates distortion at extremes of the elevational gradient, over- and under-predicting samples (Kemp and Telford, 2015). This is negated in a WA-PLS approach, which exploits the residual correlations in the modern training set which are left over after a WA model (Kemp and Telford, 2015). After the WA approach, the PLS addition employs the residuals which improves the resultant relationship.

The MAT technique does not utilize a direct species to environment relationship but rather is a numerical calculation of dissimilarity between a modern and down-core sample. Utilized here, the LWWA method specifies the number of modern samples to be included in a training set for each down-core sample. An advantage of this approach is that a large number of samples can be utilized.

d. Regression

The relationship between the elevation of the samples and the relative abundances of foraminifera is empirically modelled by regression. This is done either by expressing the foraminiferal data as a function of elevation (the classical approach) or vice versa (the inverse approach) (Horton and Edwards, 2006). At Sand Hill Point the inverse approach was chosen. The inverse approach tends to perform best when considering samples from the middle of the environmental gradient. This is the ideal approach for Sand Hill Point considering the low elevational range (~0.11 m) resulting in foraminiferal assemblages generally dominated by typical middle-marsh assemblages.

e. Calibration

The down-core foraminiferal assemblages are calibrated in order to produce estimates of paleomarsh elevation. The calibration process includes a number of inherent assumptions including: elevation remains the dominant control on foraminiferal distributions and other environmental variables do not exert a strong or changeable influence through time, and that the composition of the modern foraminiferal assemblages are representative of those found in the sub-surface (Edwards and Horton, 2006). Calibration is achieved using the C2 program in order to obtain standardized water level index (SWLI) values.

f. Standardized water level index

Sites with varying tidal ranges are often compared. Therefore, the elevations of samples need to be standardized. The processes of converting the elevation of each sample to a standardized water level index (SWLI) is accomplished using an equation relating the elevation of a sample to the water level. For sea-level reconstructions, Horton and Edwards (2006) provided the equation:

$$\mathrm{SWLI} = \frac{\mathrm{Alt}_{ab} - \mathrm{MLWS}}{\mathrm{MHWST}_b - \mathrm{MLWST}_b}$$

Where Alt_{ab} is the elevation of sample at site a; $\mathrm{MLWST_b}$ is the mean low water spring tide level at site b; and $\mathrm{MHWST_b}$ is the mean high water spring tide at site b; measured in meters (Horton and Edwards, 2006). This SWLI equation relates the sample elevation to mean high water spring tide mean low water spring tide. However, variations of SWLI utilizing different tidal parameters can be used (Horton and Edwards, 2006) but data availability allowed for Sand Hill Point SWLI values to be calculated using MHHW (mean higher high water) and MTL (mean tide level).

g. Cross-validation

Evaluating the performance of the transfer function involves cross-validating the data by simulating new data from the modern training set (Kemp and Telford, 2015). Common methods for accomplishing this include Leave-one-out (LOO) and, utilized here, bootstrapping. This method selects a fixed number of samples (e.g., n = 1000) with replacement in order to generate a new training set (Kemp and Telford, 2015).